Supplementary material

The following supplementary material is available for this article online:

Fig. S1 Semi-quantitative analysis of Hsp105 levels in the spinal cord of SOD1G93A mice.

This material is available as part of the online article from http://www.blackwell-synergy.com.

References

Andersen P. M., Forsgren L., Binzer M. *et al.* (1996) Autosomal recessive adult-onset amyotrophic lateral sclerosis associated with homozygosity for Asp90Ala CuZn-superoxide dismutase mutation. A clinical and genealogical study of 36 patients. *Brain* **119**(Pt. 4), 1153–1172.

Anttonen A. K., Mahjneh I., Hamalainen R. H. *et al.* (2005) The gene disrupted in Marinesco-Sjogren syndrome encodes SIL1, an HSPA5 cochaperone. *Nat. Genet.* **37**, 1309–1311.

Batulan Z., Shinder G. A., Minotti S., He B. P., Doroudchi M. M., Nalbantoglu J., Strong M. J. and Durham H. D. (2003) High threshold for induction of the stress response in motor neurons is associated with failure to activate HSF1. *J. Neurosci.* **23**, 5789–5798.

Bendotti C. and Carri M. T. (2004) Lessons from models of SOD1-linked familial ALS. *Trends Mol. Med.* **10**, 393–400.

Boillee S., Yamanaka K., Lobsiger C. S., Copeland N. G., Jenkins N. A., Kassiotis G., Kollias G. and Cleveland D. W. (2006) Onset and progression in inherited ALS determined by motor neurons and microglia. *Science* **312**, 1389–1392.

Bruening W., Roy J., Giasson B., Figlewicz D. A., Mushynski W. E. and Durham H. D. (1999) Up-regulation of protein chaperones preserves viability of cells expressing toxic Cu/Zn-superoxide dismutase mutants associated with amyotrophic lateral sclerosis. *J. Neurochem.* **72**, 693–699.

Bruijn L. I., Becher M. W., Lee M. K. *et al.* (1997) ALS-linked SOD1 mutant G85R mediates damage to astrocytes and promotes rapidly progressive disease with SOD1-containing inclusions. *Neuron* **18**, 327–338.

Bruijn L. I., Houseweart M. K., Kato S., Anderson K. L., Anderson S. D., Ohama E., Reaume A. G., Scott R. W. and Cleveland D. W. (1998) Aggregation and motor neuron toxicity of an ALS-linked SOD1 mutant independent from wild-type SOD1. *Science* **281**, 1851–1854.

Bruijn L. I., Miller T. M. and Cleveland D. W. (2004) Unraveling the mechanisms involved in motor neuron degeneration in ALS. *Annu. Rev. Neurosci.* **27**, 723–749.

Buchberger A., Theyssen H., Schroder H., McCarty J. S., Virgallita G., Milkereit P., Reinstein J. and Bukau B. (1995) Nucleotide-induced conformational changes in the ATPase and substrate binding domains of the DnaK chaperone provide evidence for interdomain communication. *J. Biol. Chem.* **270**, 16 903–16 910.

Choi J. S., Cho S., Park S. G., Park B. C. and Lee D. H. (2004) Co-chaperone CHIP associates with mutant Cu/Zn-superoxide dismutase proteins linked to familial amyotrophic lateral sclerosis and promotes their degradation by proteasomes. *Biochem. Biophys. Res. Commun.* **321**, 574–583.

Clement A. M., Nguyen M. D., Roberts E. A. *et al.* (2003) Wild-type nonneuronal cells extend survival of SOD1 mutant motor neurons in ALS mice. *Science* **302**, 113–117.

Dragovic Z., Broadley S. A., Shomura Y., Bracher A. and Hartl F. U. (2006) Molecular chaperones of the Hsp110 family act as nucleotide exchange factors of Hsp70s. *EMBO J.* **25**, 2519–2528.

Hand C. K., Mayeux-Portas V., Khoris J., Briolotti V., Clavelou P., Camu W. and Rouleau G. A. (2001) Compound heterozygous D90A and D96N SOD1 mutations in a recessive amyotrophic lateral sclerosis family. *Ann. Neurol.* **49**, 267–271.

Hatayama T., Yamagishi N., Minobe E. and Sakai K. (2001) Role of hsp105 in protection against stress-induced apoptosis in neuronal PC12 cells. *Biochem. Biophys. Res. Commun.* **288**, 528–534.

Hylander B. L., Chen X., Graf P. C. and Subjeck J. R. (2000) The distribution and localization of hsp110 in brain. *Brain Res.* **869**, 49–55.

Ishihara K., Yamagishi N., Saito Y., Adachi H., Kobayashi Y., Sobue G., Ohtsuka K. and Hatayama T. (2003) Hsp105alpha suppresses the aggregation of truncated androgen receptor with expanded CAG repeats and cell toxicity. *J. Biol. Chem.* **278**, 25 143–25 150.

Jensen O. N., Podtelejnikov A. and Mann M. (1996) Delayed extraction improves specificity in database searches by matrix-assisted laser desorption/ionization peptide maps. *Rapid Commun. Mass Spectrom.* **10**, 1371–1378.

Johnston J. A., Dalton M. J., Gurney M. E. and Kopito R. R. (2000) Formation of high molecular weight complexes of mutant Cu, Zn-superoxide dismutase in a mouse model for familial amyotrophic lateral sclerosis. *Proc. Natl Acad. Sci. USA* **97**, 12 571–12 576.

Jonsson P. A., Ernhill K., Andersen P. M., Bergemalm D., Brannstrom T., Gredal O., Nilsson P. and Marklund S. L. (2004) Minute quantities of misfolded mutant superoxide dismutase-1 cause amyotrophic lateral sclerosis. *Brain* **127**, 73–88.

Kato S., Takikawa M., Nakashima K., Hirano A., Cleveland D. W., Kusaka H., Shibata N., Kato M., Nakano I. and Ohama E. (2000) New consensus research on neuropathological aspects of familial amyotrophic lateral sclerosis with superoxide dismutase 1 (SOD1) gene mutations: inclusions containing SOD1 in neurons and astrocytes. *Amyotroph. Lateral Scler. Other Motor Neuron Disord.* **1**, 163–184.

Katsuno M., Sang C., Adachi H., Minamiyama M., Waza M., Tanaka F., Doyu M. and Sobue G. (2005) Pharmacological induction of heat-shock proteins alleviates polyglutamine-mediated motor neuron disease. *Proc. Natl Acad. Sci. USA* **102**, 16 801–16 806.

Kieran D., Kalmar B., Dick J. R., Riddoch-Contreras J., Burnstock G. and Greensmith L. (2004) Treatment with arimoclomol, a coinducer of heat shock proteins, delays disease progression in ALS mice. *Nat. Med.* **10**, 402–405.

Kostic V., Gurney M. E., Deng H. X., Siddique T., Epstein C. J. and Przedborski S. (1997) Midbrain dopaminergic neuronal degeneration in a transgenic mouse model of familial amyotrophic lateral sclerosis. *Ann. Neurol.* **41**, 497–504.

Lee-Yoon D., Easton D., Murawski M., Burd R. and Subjeck J. R. (1995) Identification of a major subfamily of large hsp70-like proteins through the cloning of the mammalian 110-kDa heat shock protein. *J. Biol. Chem.* **270**, 15 725–15 733.

Liu J., Shinobu L. A., Ward C. M., Young D. and Cleveland D. W. (2005) Elevation of the Hsp70 chaperone does not effect toxicity in mouse models of familial amyotrophic lateral sclerosis. *J. Neurochem.* **93**, 875–882.

Maatkamp A., Vlug A., Haasdijk E., Troost D., French P. J. and Jaarsma D. (2004) Decrease of Hsp25 protein expression precedes degeneration of motoneurons in ALS-SOD1 mice. *Eur. J. Neurosci.* **20**, 14–28.

McCarty J. S., Buchberger A., Reinstein J. and Bukau B. (1995) The role of ATP in the functional cycle of the DnaK chaperone system. *J. Mol. Biol.* **249**, 126–137.

Miyazaki K., Fujita T., Ozaki T. *et al.* (2004) NEDL1, a novel ubiquitin-protein isopeptide ligase for dishevelled-1, targets mutant superoxide dismutase-1. *J. Biol. Chem.* **279**, 11 327–11 335.

Niwa J., Ishigaki S., Hishikawa N., Yamamoto M., Doyu M., Murata S., Tanaka K., Taniguchi N. and Sobue G. (2002) Dorfin ubiquitylates mutant SOD1 and prevents mutant SOD1-mediated neurotoxicity. *J. Biol. Chem.* **277**, 36 793–36 798.

Oeda T., Shimohama S., Kitagawa N., Kohno R., Imura T., Shibasaki H. and Ishii N. (2001) Oxidative stress causes abnormal accumulation of familial amyotrophic lateral sclerosis-related mutant SOD1 in transgenic Caenorhabditis elegans. *Hum. Mol. Genet.* **10**, 2013–2023.

Oh H. J., Chen X. and Subjeck J. R. (1997) Hsp110 protects heat-denatured proteins and confers cellular thermoresistance. *J. Biol. Chem.* **272**, 31 636–31 640.

Oh H. J., Easton D., Murawski M., Kaneko Y. and Subjeck J. R. (1999) The chaperoning activity of hsp110. Identification of functional domains by use of targeted deletions. *J. Biol. Chem.* **274**, 15 712–15 718.

Okado-Matsumoto A. and Fridovich I. (2002) Amyotrophic lateral sclerosis: a proposed mechanism. *Proc. Natl Acad. Sci. USA* **99**, 9010–9014.

Parton M. J., Andersen P. M., Broom W. J. and Shaw C. E. (2001) Compound heterozygosity and variable penetrance in SOD1 amyotrophic lateral sclerosis pedigrees. *Ann. Neurol.* **50**, 553–554.

Raviol H., Sadlish H., Rodriguez F., Mayer M. P. and Bukau B. (2006) Chaperone network in the yeast cytosol: Hsp110 is revealed as an Hsp70 nucleotide exchange factor. *EMBO J.* **25**, 2510–2518.

Rudiger S., Buchberger A. and Bukau B. (1997) Interaction of Hsp70 chaperones with substrates. *Nat. Struct. Biol.* **4**, 342–349.

Senderek J., Krieger M., Stendel C. *et al.* (2005) Mutations in SIL1 cause Marinesco-Sjogren syndrome, a cerebellar ataxia with cataract and myopathy. *Nat. Genet.* **37**, 1312–1314.

Shinder G. A., Lacourse M. C., Minotti S. and Durham H. D. (2001) Mutant Cu/Zn-superoxide dismutase proteins have altered solubility and interact with heat shock/stress proteins in models of amyotrophic lateral sclerosis. *J. Biol. Chem.* **276**, 12 791–12 796.

Urushitani M., Kurisu J., Tateno M., Hatakeyama S., Nakayama K., Kato S. and Takahashi R. (2004) CHIP promotes proteasomal degradation of familial ALS-linked mutant SOD1 by ubiquitinating Hsp/Hsc70. *J. Neurochem.* **90**, 231–244.

Vleminckx V., Van Damme P., Goffin K., Delye H., Van Den Bosch L. and Robberecht W. (2002) Upregulation of HSP27 in a transgenic model of ALS. *J. Neuropathol. Exp. Neurol.* **61**, 968–974.

Wang J., Xu G. and Borchelt D. R. (2002a) High molecular weight complexes of mutant superoxide dismutase 1: age-dependent and tissue-specific accumulation. *Neurobiol. Dis.* **9**, 139–148.

Wang J., Xu G., Gonzales V., Coonfield M., Fromholt D., Copeland N. G., Jenkins N. A. and Borchelt D. R. (2002b) Fibrillar inclusions and motor neuron degeneration in transgenic mice expressing superoxide dismutase 1 with a disrupted copper-binding site. *Neurobiol. Dis.* **10**, 128–138.

Wang J., Slunt H., Gonzales V., Fromholt D., Coonfield M., Copeland N. G., Jenkins N. A. and Borchelt D. R. (2003) Copper-binding-site-null SOD1 causes ALS in transgenic mice: aggregates of non-native SOD1 delineate a common feature. *Hum. Mol. Genet.* **12**, 2753–2764.

Watanabe M., Dykes-Hoberg M., Culotta V. C., Price D. L., Wong P. C. and Rothstein J. D. (2001) Histological evidence of protein aggregation in mutant SOD1 transgenic mice and in amyotrophic lateral sclerosis neural tissues. *Neurobiol. Dis.* **8**, 933–941.

Yamagishi N., Ishihara K., Saito Y. and Hatayama T. (2003) Hsp105 but not Hsp70 family proteins suppress the aggregation of heat-denatured protein in the presence of ADP. *FEBS Lett.* **555**, 390–396.

Yasuda K., Nakai A., Hatayama T. and Nagata K. (1995) Cloning and expression of murine high molecular mass heat shock proteins, HSP105. *J. Biol. Chem.* **270**, 29 718–29 723.

Cell

Homeostatic Levels of p62 Control Cytoplasmic Inclusion Body Formation in Autophagy-Deficient Mice

Masaaki Komatsu,[1,2,3] Satoshi Waguri,[4] Masato Koike,[5] Yu-shin Sou,[1,2] Takashi Ueno,[2] Taichi Hara,[6] Noboru Mizushima,[6,7] Jun-ichi Iwata,[1,2] Junji Ezaki,[2] Shigeo Murata,[1] Jun Hamazaki,[1] Yasumasa Nishito,[1] Shun-ichiro Iemura,[8] Tohru Natsume,[8] Toru Yanagawa,[9] Junya Uwayama,[9] Eiji Warabi,[9] Hiroshi Yoshida,[9] Tetsuro Ishii,[9] Akira Kobayashi,[10] Masayuki Yamamoto,[10] Zhenyu Yue,[11] Yasuo Uchiyama,[5] Eiki Kominami,[2] and Keiji Tanaka[1,*]

[1]Laboratory of Frontier Science, Tokyo Metropolitan Institute of Medical Science, Bunkyo-ku, Tokyo 113-8613, Japan
[2]Department of Biochemistry, Juntendo University School of Medicine, Bunkyo-ku, Tokyo 113-8421, Japan
[3]PRESTO, Japan Science and Technology Corporation, Kawaguchi 332-0012, Japan
[4]Department of Anatomy and Histology, Fukushima Medical University School of Medicine, Hikarigaoka, Fukushima 960-1295, Japan
[5]Department of Cell Biology and Neurosciences, Osaka University Graduate School of Medicine, Suita, Osaka 565-0871, Japan
[6]Department of Physiology and Cell Biology, Tokyo Medical and Dental University Graduate School and Faculty of Medicine, Bunkyo-ku, Tokyo 113-8519, Japan
[7]SORST, Japan Science and Technology Corporation, Kawaguchi 332-0012, Japan
[8]National Institutes of Advanced Industrial Science and Technology, Biological Information Research Center (JBIRC), Kohtoh-ku, Tokyo 135-0064, Japan
[9]Graduate School of Comprehensive Human Sciences, University of Tsukuba, Tennoudai, Tsukuba 305-8575, Japan
[10]Department of Medical Biochemistry and ERATO-JST, Tohoku University Graduate School of Medicine, Aoba-ku, Sendai 980-8575, Japan
[11]Departments of Neurology and Neuroscience, Mount Sinai School of Medicine, New York, NY 10029, USA
*Correspondence: tanakak@rinshoken.or.jp
DOI 10.1016/j.cell.2007.10.035

SUMMARY

Inactivation of constitutive autophagy results in formation of cytoplasmic protein inclusions and leads to liver injury and neurodegeneration, but the details of abnormalities related to impaired autophagy are largely unknown. Here we used mouse genetic analyses to define the roles of autophagy in the aforementioned events. We report that the ubiquitin- and LC3-binding protein "p62" regulates the formation of protein aggregates and is removed by autophagy. Thus, genetic ablation of *p62* suppressed the appearance of ubiquitin-positive protein aggregates in hepatocytes and neurons, indicating that p62 plays an important role in inclusion body formation. Moreover, loss of *p62* markedly attenuated liver injury caused by autophagy deficiency, whereas it had little effect on neuronal degeneration. Our findings highlight the unexpected role of homeostatic level of p62, which is regulated by autophagy, in controlling intracellular inclusion body formation, and indicate that the pathologic process associated with autophagic deficiency is cell-type specific.

INTRODUCTION

Macroautophagy (hereafter referred to as autophagy) is a highly conserved bulk protein degradation pathway in eukaryotes. In the initial step of this process, the cytoplasmic portions and organelles are engulfed within a double-membrane vesicle called autophagosome, and then the autophagosome fuses with the lysosomes to degrade the sequestered materials by various lysosomal hydrolytic enzymes, followed by generation of amino acids that are recycled for macromolecular synthesis and energy production. Emerging evidence emphasizes the importance of autophagy in various biological and pathological processes, such as cellular remodeling, tumorigenesis, and developmental programs (Levine and Klionsky, 2004).

Recent evidence indicates that in mammalian cells, autophagy serves two physiological purposes. The first is to supply amino acids for cell survival under poor environmental conditions, which is universally known as "adaptive autophagy." Indeed, this type of autophagy is rapidly induced under nutritional deprivation in yeast (Tsukada and Ohsumi, 1993) and in newborn mice (Kuma et al., 2004), serving as a basic survival strategy in all eukaryotes. The second is to degrade proteins in the cell through continuous operation at a low level irrespective of nutritional stress, known as "basal or constitutive autophagy." In the latter pathway, autophagy is responsible for the

turnover of long-lived proteins, disposal of excess (Iwata et al., 2006) or damaged organelles (Elmore et al., 2001), and clearance of aggregate-prone proteins (Fortun et al., 2003; Kamimoto et al., 2006; Ravikumar et al., 2004). Recent genetic studies using mice have highlighted the importance of constitutive autophagy in nondividing cells, such as hepatocytes and neurons, in which loss of autophagy results in severe liver injury and neurodegeneration, respectively (Hara et al., 2006; Komatsu et al., 2005, 2006). Unexpected findings in these studies were that loss of autophagy causes cytoplasmic accumulation of ubiquitin-positive proteinaceous inclusions, together with hepatocytic and neuronal death without expression of proteins with disease-associated mutations (Hara et al., 2006; Komatsu et al., 2005, 2006). However, the underlying mechanism of inclusion body formation in the aforementioned diseases is largely unknown at present.

Using mouse genetics, we report the critical role of the multifunctional protein "p62/A170/SQSTM1" (also known as a signaling adaptor/scaffold protein) in the formation of intracellular ubiquitin-related protein aggregation caused by deficiency in autophagy. We show that autophagic degradation of the "p62" via direct interaction with LC3, a posttranslational modifier essential for autophagosome formation, prevents inclusion body formation. Importantly, our studies uncover the molecular mechanism linking autophagy, p62, and inclusion body formation, which is a cellular hallmark in various pathophysiological conditions, and reveal pathophysiological changes associated with loss of p62 and/or autophagy in hepatocytes and neurons.

RESULTS

Identification of LC3-Interacting Proteins

The microtubule-associated protein 1A/1B *l*ight chain *3* (LC3) is a modifier protein conjugated with phosphatidylethanolamine (PE), analogous to Atg8 in yeast (Ichimura et al., 2000). PE-conjugated LC3 (LC3-II) is localized in the inner and outer membranes of autophagosomes, and the population associated with the inner membrane is degraded after fusion of autophagosomes with lysosomes (Kabeya et al., 2000). To identify protein(s) that could interact with LC3, we employed the proteomic approach as described previously (Komatsu et al., 2004) and then identified a unique protein p62 as one of LC3-interacting proteins, in addition to LC3-modifying enzymes (Ohsumi, 2001) (Table S1). The p62 protein is conserved in metazoa and plants but not in yeasts and can bind a large number of proteins through its multiple protein-protein interaction motifs (Moscat et al., 2006) (Figure S1). This protein mediates diverse signaling pathways including cell stress, survival, and inflammation (Moscat et al., 2006; Wooten et al., 2006).

p62 Is Degraded by Autophagy-Lysosome Pathway

To verify the interaction between LC3 and p62 in vivo, we first carried out immunoprecipitation assay with cultured hepatocytes isolated from green fluorescent protein (GFP)-LC3 transgenic (Tg) mice (GFP-LC3 tg) (Mizushima et al., 2004) and confirmed the coimmunoprecipitation of p62 with GFP-LC3 under both nutrient-rich and -poor conditions (Figure 1A). We also confirmed the coimmunoprecipitation of p62 with endogenous LC3 in wild-type mouse liver (Figure 1B). In addition to the major band, the minor band detected by our p62 antibody was probably a p62 splicing variant product found in the mouse protein database or a partially cleaved product (see also Figures 2, 3, and 4). Moreover, recombinant p62 was pulled down with recombinant GST-LC3 (Figure 1C), indicating direct physical interaction between p62 and LC3. Subsequent binding assays with a series of recombinant p62 mutants indicated that p62 interacts with LC3 through a linker region that connects the N-terminal Zinc finger and the C-terminal *ub*iquitin-*a*ssociated (UBA) domain of p62 (Figure S1). Immunofluorescence microscopy using hepatocytes isolated from GFP-LC3 Tg mice showed colocalization of large numbers of punctate signal for GFP-LC3 (84.7% ± 10.9%, ± SD, n = 21) with that for p62 (Figure 1E). When autophagosome formation was induced by nutrient-deprivation, 34.9% ± 6.7% (n = 22) of ring-shaped GFP-LC3-positive autophagosomes contained p62 signal, some of which showed partial colocalization (Figure 1F). A similar colocalization pattern was also observed in liver sections of GFP-LC3 Tg starved for 1 day (Figure 1G). The p62-positive and GFP-LC3-negative particles might correspond to late endosomes or lysosomes, as reported previously (Sanchez et al., 1998). Consistent with the notion that some population of LC3-II is degraded in lysosomes (Kabeya et al., 2000), treatment with lysosomal enzyme inhibitors, but not with a proteasomal inhibitor, resulted in the accumulation of LC3-II in primary hepatocytes (Figure 1D). Similarly, lysosomal inhibition resulted in marked accumulation of p62 (Figure 1D). When lysosomal inhibitors were added to cultured hepatocytes, the majority of p62 accumulated around the perinuclear region, where it colocalized with the lysosomal marker LysoTracker (Figure 1H), suggesting the turnover of p62 together with LC3II in lysosomes.

p62 Is a Component of Inclusions in Autophagy-Deficient Hepatocytes

If p62 is degraded by the autophagic-lysosome pathway, autophagy deficiency should result in the accumulation of p62 protein. To test this in vivo, we used the *Atg7*$^{F/F}$:Mx1 mice, in which *Atg7*, a gene essential for autophagy, can be depleted in the liver by intraperitoneal injections of polyinosinic acid-polycytidylic acid (pIpC) (Figure 2A, left panel) (Komatsu et al., 2005). We observed specific accumulation of p62 protein in *Atg7*-deficient livers (Figures 2A and 2D) without marked induction of p62 mRNA (Figure 2E). Similar to *Atg7* knockout liver, deficiency of *Atg5*, which is essential for autophagosome formation (Mizushima et al., 2001), was also associated with marked accumulation of p62 (Figure S2). These results indicate that p62 turnover is mediated by autophagy. Autophagic

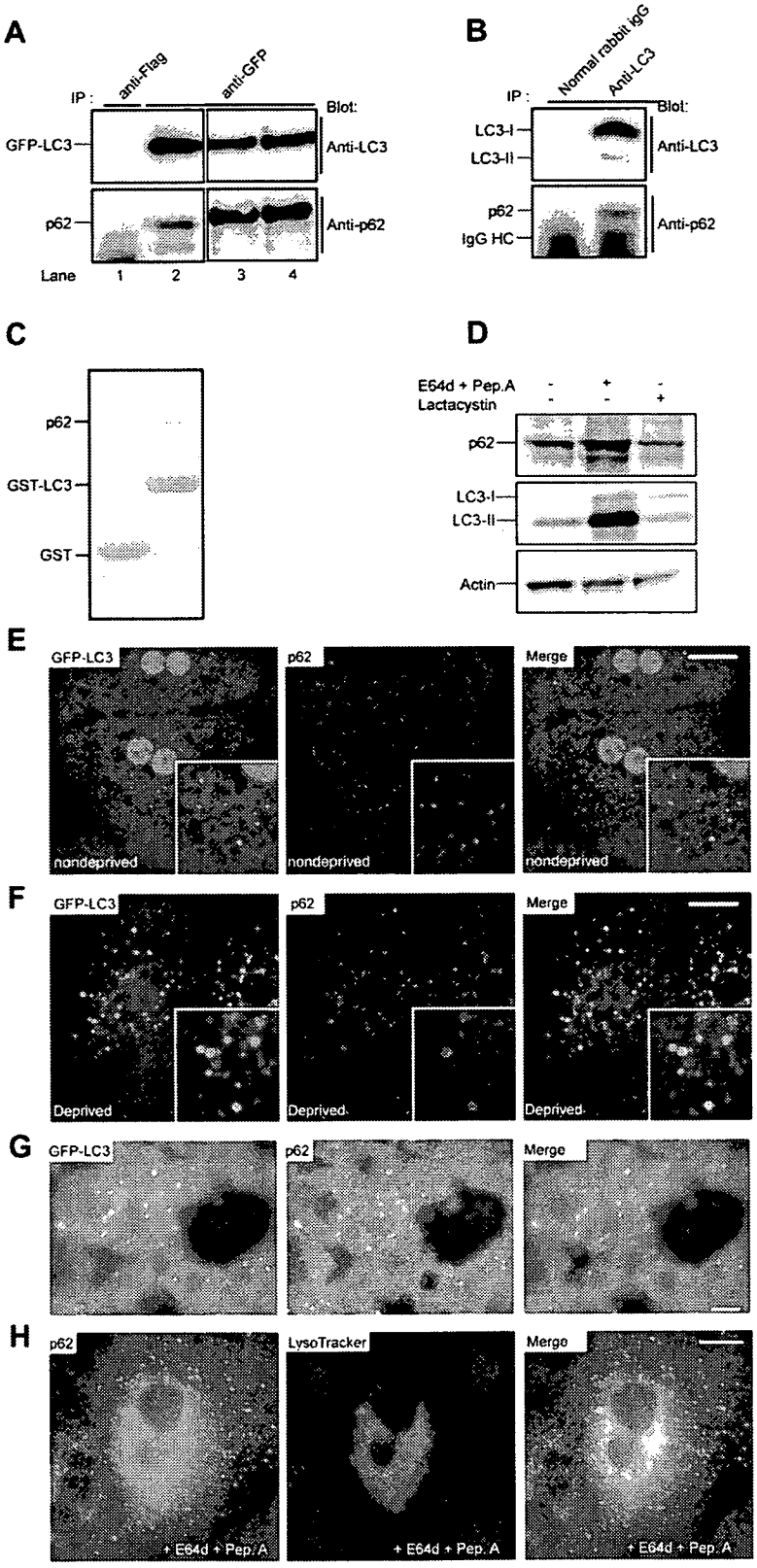

Figure 1. p62 Is Degraded by the Autophagic-Lysosomal Pathway

(A) Interaction of p62 with GFP-LC3. Hepatocytes prepared from GFP-LC3 Tg mice were cultured for 3 hr in Williams' E medium (lanes 1, 2, and 3) or Hank's solution (lane 4). The cell lysates were immunoprecipitated with anti-Flag or GFP antibodies followed by immunoblotting with antibodies against LC3 and p62.

(B) Interaction of p62 with endogenous LC3. Liver lysates from wild-type mice were immunoprecipitated with anti-LC3 antibody or normal rabbit IgG followed by immunoblotting with antibodies against LC3 and p62.

(C) In vitro GST pull-down analysis of purified p62 by recombinant GST or GST-LC3.

(D) Degradation of p62 and LC3. Hepatocytes prepared from wild-type mice were treated with E64d (10 μg/ml) and pepstatin A (10 μg/ml) for 24 hr or lactacystin (10 μM) for 3 hr. The cell lysates were subjected to SDS-PAGE followed by immunoblotting with indicated antibodies. Data shown in (A)–(D) are representative of three separate experiments.

(E, F, and H) Immunofluorescent analysis of primary cultured hepatocytes. Hepatocytes isolated from GFP-LC3 Tg mice were cultured for 3 hr in Williams' E medium (E) and Hank's solution (F) or for 24 hr in Williams' E with E64d and pepstatin A (H) and then immunostained with antibody against p62. Lysosomal inhibitor-treated hepatocytes were stained with the fluorescent acidotropic probe LysoTracker prior to p62 immunostaining (H). Higher magnification views are shown in insets. Bar, 10 μm.

(G) Immunofluorescence analysis of the liver of GFP-LC3 Tg mice. Mice were fasted for 1 day, and then the liver sections were immunostained with anti-p62 antibody. Right panels show merged images. Bar, 10 μm.

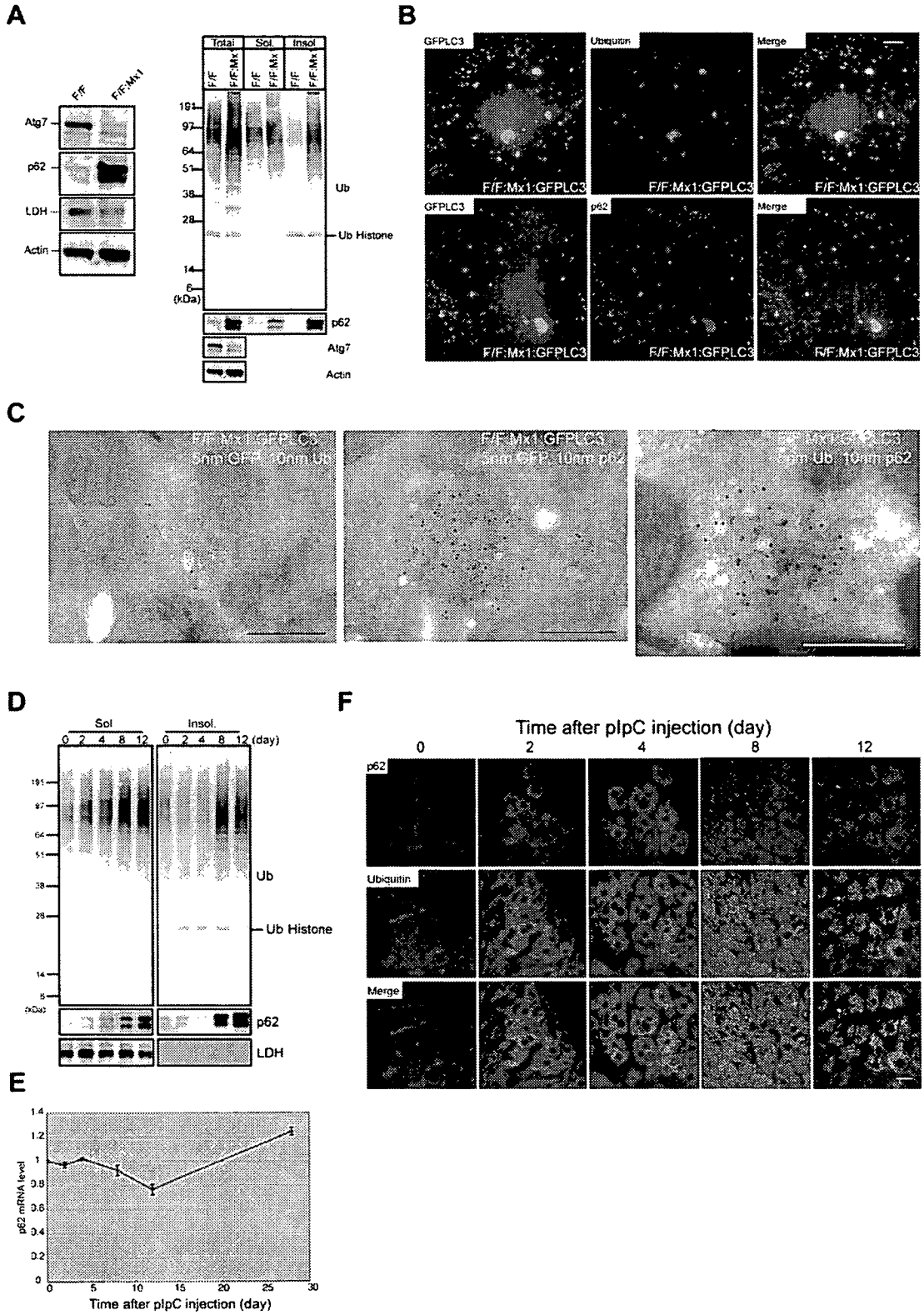

Figure 2. Formation of Ubiquitin- and p62-Positive Inclusions in Autophagy-Deficient Hepatocytes

(A) Accumulation of p62 in *Atg7*-deficient hepatocytes. Left panel shows liver homogenates from *Atg7*$^{F/F}$ and *Atg7*$^{F/F}$:Mx1 mice at 28-day post-pIpC injection were subjected to SDS-PAGE followed by immunoblotting with indicated antibodies. Right panel shows liver homogenates were separated

breakdown of p62 appears to occur irrespective of cell type, because a similar observation was recently reported in HeLa, HEK293T, and mouse embryonic fibroblasts (Bjorkoy et al., 2005; Wang et al., 2006).

Interestingly, abundant amounts of p62 were noted in both detergent-soluble and insoluble fractions from *Atg7*-deficient livers (Figure 2A, right-middle panel), in parallel with accumulation of ubiquitinated proteins in both fractions from *Atg7*-deficient but not from control livers (Figure 2A, right-top panel) (Komatsu et al., 2005). Subsequently, to investigate the cellular localization of ubiquitin, p62, and LC3 in autophagy-deficient hepatocytes, we generated the $Atg7^{F/F}$:Mx1:GFP-LC3 mice by crossing $Atg7^{F/F}$:Mx1 with GFP-LC3 Tg mice. Immunofluorescence microscopy showed that the *Atg7*-deficient cultured hepatocytes contained abundant ubiquitin- (Figure 2B, top panels), or p62- (Figure 2B, bottom panels) positive inclusions in the cytoplasm, which were also positive for GFP-LC3. Finally, double immunoelectron microscopy confirmed the colocalization of LC3, ubiquitin, and p62 proteins in the cytoplasmic aggregated structures (Figures 2C and S3). Next, we analyzed the inclusion formation process. Immunoblot analysis revealed that p62 began to accumulate in the detergent-soluble fraction at 4 days and was abundant in both detergent-soluble and -insoluble fractions at 8 days (Figure 2D). In contrast, RT-PCR analysis showed no induction of p62 transcript during this period (Figure 2E). The accumulation pattern of polyubiquitinated proteins essentially matched that of p62 (Figure 2D). Double-immunofluorescence microscopy showed the appearance of ubiquitin- and p62-double-positive dots at 2 days in some $Atg7^{F/F}$:Mx1 hepatocytes (Figure 2F). At later stages, both the number of hepatocytes containing the inclusions and the size of the inclusions increased gradually with time. These results suggest the time-dependent development of inclusions containing both ubiquitin and p62 in autophagy-deficient hepatocytes.

p62 Is a Component of Inclusions in Autophagy-Deficient Neurons

Next, we investigated the behavior of p62 in neuronal-specific autophagy-deficient mice, $Atg7^{F/F}$:Nes mice (Komatsu et al., 2006). Similar to autophagy-deficient livers, p62 accumulated in the mutant brain without the apparent induction of its mRNA (Figures 3A and 3B), implying a common pathway in p62 turnover across tissues. Furthermore, the p62-positive inclusions were observed immunohistochemically in various brain regions in $Atg7^{F/F}$:Nes mice (Figure S4). Double-immunofluorescence microscopy revealed extensive colocalization of p62 and LC3 (Figure 3C, left panels), or p62 and ubiquitin (Figure 3C, right panels), in numerous inclusions in the cerebral cortex. Immunoelectron microscopy confirmed the localization of p62 in the cytoplasmic aggregated structures (Figures 3D, top panel, and S5). These inclusions also contained ubiquitin (Figures 3D, bottom panel, and S5). Next, we investigated the time course of inclusion formation in the cerebral cortex of $Atg7^{F/F}$:Nes mice from 2 to 28 days after birth. Ubiquitin/p62-double-positive dots began to appear at postnatal day 2 in the cerebral cortex, and they increased in size and number during postnatal development (Figure 3E). Taken together, these results indicate that reduced autophagic activity leads to the formation of ubiquitin- and p62-double positive inclusions in neurons.

Generation of *p62*-Knockout Mice

To examine the physiological roles of p62 in autophagy, we generated *p62*-knockout ($p62^{-/-}$) mice (Figure S6). They were born at Mendelian frequency, fertile and lived longer than 1 year (data not shown). Although *p62* deficiency was associated with adulthood-onset obesity and diabetes as reported recently (Rodriguez et al., 2006), no apparent abnormality was noted in the *p62*-deleted liver (Figure S7). Moreover, *p62*-deficient mice exhibited neither marked neurodegeneration nor inclusion formation in neurons (see Figures 6 and S8). The conversion from LC3-I to LC3-II, induction of GFP-LC3 dots, and the appearance of many autophagosome structures after starvation were similar between the control and *p62*-deficient hepatocytes (Figures S9A, S9B, and S9C). Furthermore, there was no significant change in the turnover of long-lived protein in the mutant hepatocytes (Figure S9D).

into detergent (0.5% Tx-100)-soluble (Sol.) and insoluble (Insol.) fractions. Each fraction was subjected to SDS-PAGE and analyzed by immunoblotting with indicated antibodies. Data shown are representative of three separate experiments.

(B) Immunofluorescence analysis of cellular localization of ubiquitin, p62, and LC3 in autophagy-deficient hepatocytes. Hepatocytes isolated from $Atg7^{F/F}$:Mx1:GFP-LC3 mice at 14-day post-pIpC injection were immunostained with anti-ubiquitin or p62 antibodies. Right panels show merged images. Bar, 10 μm.

(C) Immunoelectron micrograph showing double labeling of ubiquitin (10 nm colloidal gold particles [cgp]) and GFP (5 nm cgp), p62 (10 nm cgp), and GFP (5 nm cgp), or p62 (10 nm cgp) and ubiquitin (5 nm cgp) in hepatocytes isolated from $Atg7^{F/F}$:Mx1:GFP-LC3 mice at 14-day post-pIpC injection. Bars, 0.5 μm. Magnified images can be seen in Figure S3.

(D) Immunoblotting analyses of ubiquitinated proteins and p62 in $Atg7^{F/F}$:Mx1 mice livers at various time points post-pIpC injection. Each fraction prepared as shown in (A) was subjected to SDS-PAGE and analyzed by immunoblotting with indicated antibodies. Data shown are representative of three separate experiments.

(E) Quantitation of p62 mRNA level in $Atg7^{F/F}$:Mx1 liver by RT-PCR. Total RNAs were prepared from $Atg7^{F/F}$:Mx1 livers at various time points post-pIpC injection, and then cDNA was synthesized from each RNA, followed by real-time PCR analysis. Data are mean ± standard deviation (SD) values of p62 mRNA normalized to the amount in $Atg7^{F/F}$:Mx1 liver at 0 day post-pIpC injection.

(F) Immunohistochemical detection of p62- and ubiquitin-positive inclusions in *Atg7*-deficient livers. $Atg7^{F/F}$:Mx1 mice were sacrificed at various time points post-pIpC injection, and liver sections were immunostained with anti-ubiquitin and p62 antibodies. Bottom panels show merged images. Bar, 10 μm.

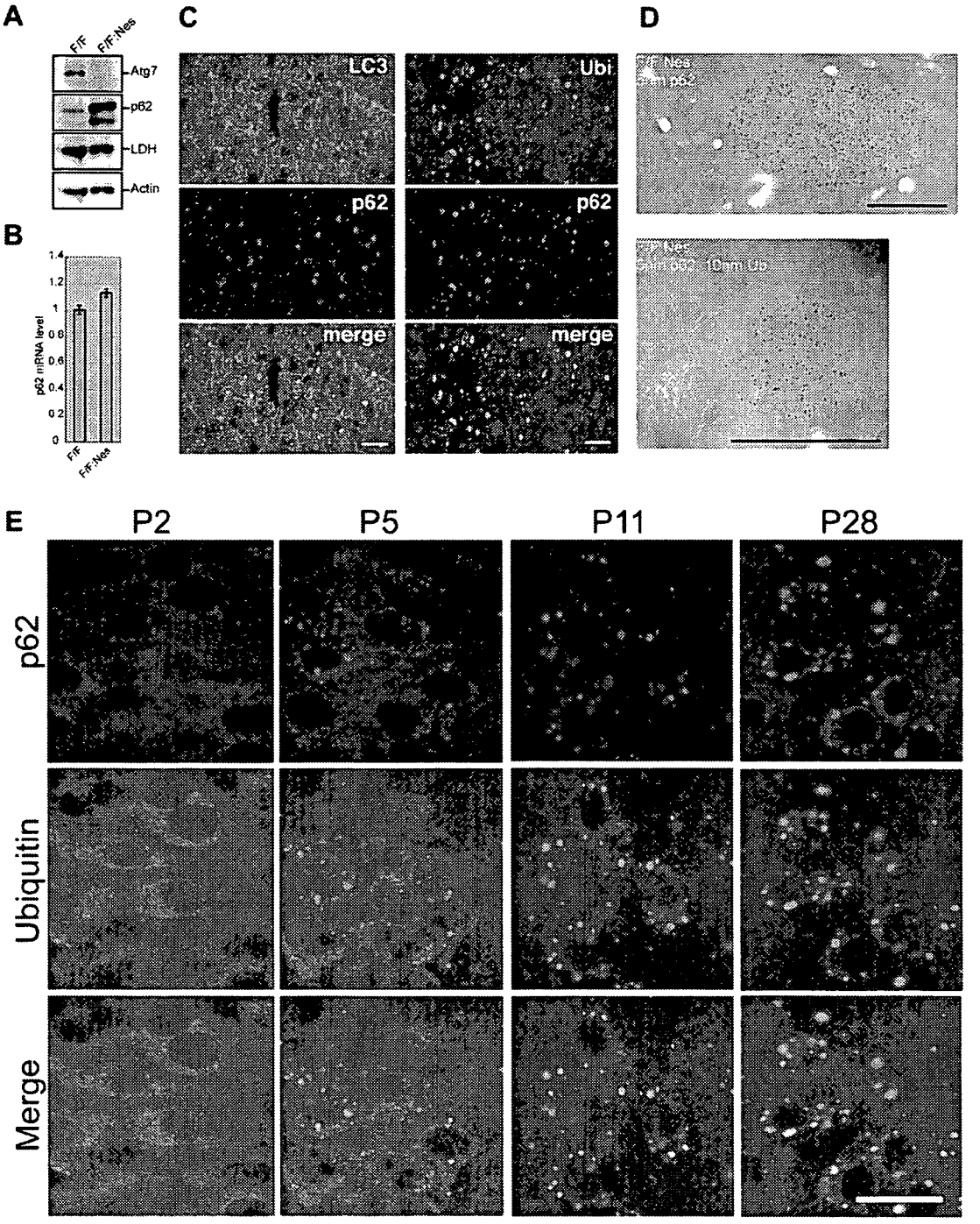

Figure 3. Formation of Ubiquitin- and p62-Positive Inclusions in Autophagy-Deficient Neurons

(A) Accumulation of p62 in *Atg7*-deficient brains. Brain homogenates from $Atg7^{F/F}$ and $Atg7^{F/F}$:Nes mice at 8 weeks of age were subjected to SDS-PAGE and analyzed by immunoblotting with indicated antibodies. Data shown are representative of three separate experiments.

(B) Quantitation of p62 mRNA level in *Atg7*-deficient brains by RT-PCR. Total RNAs were prepared from brains of $Atg7^{F/F}$ and $Atg7^{F/F}$:Nes mice at 8 weeks of age and analyzed as shown in Figure 2E. Data are mean ± SD values of p62 mRNA normalized to the amount in $Atg7^{F/F}$ brain. The experiments were performed three times.

(C) Immunofluorescence microscopy in $Atg7^{F/F}$:Nes cerebral cortex. Brain sections of $Atg7^{F/F}$:Nes mice were immunostained with anti-LC3 and p62 antibodies (left panels) or anti-ubiquitin and p62 antibodies (right panels). Bottom panels show merged images. Bar, 10 μm.

(D) Immunoelectron micrograph showing labeling of p62 (top panel) or double labeling of ubiquitin (10 nm cgp) and p62 (5 nm cgp) in hypothalamic neurons of 8-week-old $Atg7^{F/F}$:Nes mice. Bars, 0.5 μm. Magnified images can be seen in Figure S5.

Loss of p62 Suppresses Inclusion Formation in Autophagy-Deficient Hepatocytes

Next, to investigate the roles of p62 in inclusion formation, we crossed *Atg7*$^{F/F}$:Mx1 with *p62*$^{-/-}$ mice, producing the *Atg7*- and *p62*-double knockout (DKO) mice (*Atg7*$^{F/F}$:Mx1:*p62*$^{-/-}$). In contrast to large number of inclusions positive for ubiquitin in *Atg7*-deficient hepatocytes, surprisingly such ubiquitin inclusions were almost completely dispersed in the DKO hepatocytes (Figure 4A). Immunoblot analysis revealed that the amounts of accumulated polyubiquitinated proteins in DKO liver were lower than those in *Atg7*-deficient liver. Moreover, the reduction was more prominent in the insoluble fraction (Figures 4B and S10A). Interestingly, proteasome function evaluated by the degradation of polyubiquitinated protein was not significantly different among the genotypes (Figure S11A). Furthermore, the degradation of long-lived protein in DKO hepatocytes was significantly reduced to the levels as shown in *Atg7*-deficient hepatocytes (Figure S11C). Electron microscopic analysis showed that the number of aggregate structures and aberrant concentric membranous structures that were typical in *Atg7*-deficient hepatocytes (Komatsu et al., 2005) were markedly reduced, whereas smooth endoplasmic reticulum and peroxisomes were still abundantly observed in DKO hepatocytes (Figure 4C).

Loss of p62 Suppresses Inclusion Formation in Autophagy-Deficient Neurons

We also examined the roles of p62 in inclusion formation in autophagy-deficient neurons. As shown in Figure S8, while no ubiquitin-positive inclusions were detected in the brains of wild-type and *p62*-knockout mice, ubiquitin-positive inclusions of various sizes were recognized immunohistochemically in several regions of the *Atg7*$^{F/F}$:Nes brain. Such inclusions were hardly detected in the *Atg7*$^{F/F}$:Nes:*p62*$^{-/-}$ (DKO) neurons (Figures 4D and S8). Unlike autophagy-deficient livers, it was difficult to convincingly detect by immunoblot analyses any differences in the amount of insoluble polyubiquitinated protein between *Atg7*- and *Atg7*/*p62*-DKO brain (Figures 4E and S10B). This discrepancy could be due to the relatively low amounts of insoluble ubiquitinated proteins in total brain lysates from *Atg7*$^{F/F}$:Nes mice, which were insufficient for the detection of the difference. Actually, the inclusions were observed in some restricted areas such as the hypothalamus and cerebral cortex, and they were hardly observed in glial cells (Hara et al., 2006; Komatsu et al., 2006). Previous electron microscopic analysis showed that the hypothalamic neurons in *Atg7*$^{F/F}$:Nes brain contained large inclusion bodies in the perikarya (Komatsu et al., 2006). Although such inclusions were hardly detected in the same region of DKO brain, we noticed the presence of several large neuritic structures with numerous pleomorphic features of smooth endoplasmic reticulum (Figure 4F; c, e, and f). Similar alteration was also observed in the *Atg7*$^{F/F}$:Nes hypothalamus (Figure 4F, b and d), but not in the control (Figure 4F, a). In the cerebellar nuclei of both *Atg7*$^{F/F}$:Nes and DKO brains, which contained abundant round eosinophilic structures as evident in hematoxylin and eosin (H&E) stained sections (Figure 6C, bottom panel), myelinated axons were frequently enlarged and contained aberrant membranous structures and/or degenerated materials (Figures S12B–S12F), suggesting axonal degeneration in both *Atg7*$^{F/F}$:Nes and DKO neurons. Taken together, these results strongly suggest that the inclusion formation but not axonal degeneration is largely dependent on the presence of p62 in autophagy-deficient neurons.

Liver Injury in Autophagy-Deficient Mice Is Suppressed by Loss of p62

To examine whether abnormalities in autophagy-deficient liver are partly caused by the accumulation of p62, we examined the phenotypes of *Atg7*$^{F/F}$:Mx1:*p62*$^{-/-}$ mice. Surprisingly, simultaneous loss of *Atg7* and *p62* in the liver significantly suppressed the deleterious phenotypes caused by ablation of autophagy (Figures 5A and 5B). Indeed, histological analysis showed hepatocytic hypertrophy in *Atg7*-deficient liver and its suppression in DKO liver. Accordingly, the hepatic lobular structure was considerably better recognized in DKO than in *Atg7*-deficient liver (Figure 5C). While serum levels of aspartate aminotransferase (AST), alanine aminotransferase (ALT), and alkaline phosphatase (ALP) were elevated in the DKO mice compared with the control mice, the levels were markedly lower than those in single *Atg7*-deficient mice (Figure 5D). Almost the same results were observed in *Atg7*$^{F/F}$:Alb:*p62*$^{-/-}$ mice, which exhibited impaired autophagy in hepatocytes at postnatal stage, without pIpC injection (Figure S13), indicating that pIpC injection itself does not affect phenotypes of *Atg7*$^{F/F}$:Mx1 or *Atg7*$^{F/F}$:Mx1:*p62*$^{-/-}$ mice. Taken together, these results indicate that excess accumulation of p62 is a major cause of the pathogenic changes seen in the liver of autophagy-deficient mice.

Ablation of *p62* Leads to Neither Improvement nor Exacerbation of the Phenotypes in Autophagy-Deficient Neurons

Further, to investigate whether defects in autophagy-deficient brain are also attributed to accumulation of p62 in neurons, we examined the phenotypes of *Atg7*$^{F/F}$:Nes:*p62*$^{-/-}$ mice. In contrast to the recovery of liver injury in *Atg7*$^{F/F}$:Mx1 mice by simultaneous loss of *p62*, ablation of *p62* did not rescue behavioral abnormalities such as tremor and abnormal limb clasping recognized in *Atg7*$^{F/F}$:Nes mice (data not shown). Furthermore, histological

(E) Appearance of p62- and ubiquitin-positive inclusions in *Atg7*-deficient cerebral cortex during postnatal (P) development. *Atg7*$^{F/F}$:Nes mice were sacrificed at P2, 5, 11, and 28 days, and the brain sections were immunostained with anti-ubiquitin and p62 antibodies. Bottom panels show merged images. Bar, 20 μm.

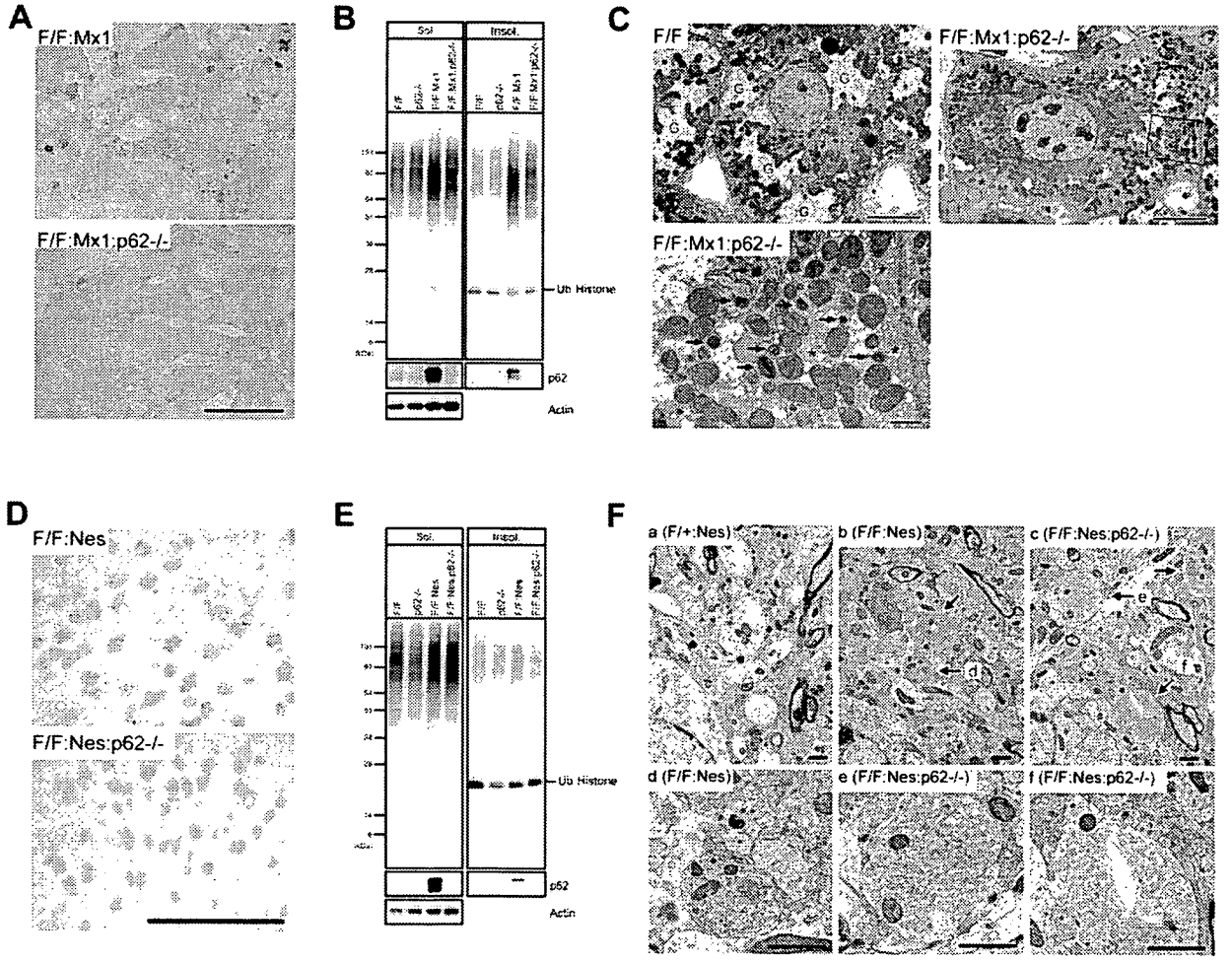

Figure 4. Indispensable Role of p62 in Inclusion Formation in Autophagy-Deficient Cells

(A) Immunohistochemical analysis of ubiquitin inclusions in *Atg7*- and *Atg7/p62*-deficient liver. Liver sections from $Atg7^{F/F}$:Mx1 and $Atg7^{F/F}$:Mx1:$p62^{-/-}$ mice at 14-day post-pIpC injection were immunostained with anti-ubiquitin antibody. Bar, 100 μm.

(B) Immunoblotting analysis of *Atg7*- and *Atg7/p62*-deficient livers. Liver homogenates from mice of the indicated genotype at 28-day post-pIpC injection were separated into detergent-soluble and insoluble fractions as shown in Figure 2. Each fraction was subjected to SDS-PAGE and analyzed by immunoblotting with indicated antibodies. Data shown are representative of three separate experiments.

(C) Electron micrographs of control and *Atg7/p62*-deficient liver. Note that the glycogen area (G), easily observed in control hepatocytes, is markedly reduced in *Atg7/p62*-deficient hepatocytes. The boxed region in the top right panel is further magnified in the bottom left panel. Asterisks indicate regions filled with smooth endoplasmic reticulum. Arrows indicate peroxisomes. Bars, 10 μm (left and right top panels) and 1 μm (left bottom panel).

(D) Immunohistochemical analysis of *Atg7*- and *Atg7/p62*-deficient brains. The presence of ubiquitin-positive particles was examined immunohistochemically in the hypothalamic regions of $Atg7^{F/F}$:Nes and $Atg7^{F/F}$:Nes:$p62^{-/-}$ mice. Bar, 100 μm.

(E) Immunoblotting analysis of *Atg7*- and *Atg7/p62*-deficient brains. Brain homogenates from mice of the indicated genotypes at 8 weeks of age were analyzed by immunoblotting as shown in (B). Data shown are representative of three separate experiments.

(F) Electron micrographs of the hypothalamus of mice of the indicated genotype. Note that several electron-lucent neuritic structures are detected in the control neuropil (a), which are only rarely seen in the *Atg7*- (b) and *Atg7/p62*-deficient (c) tissues. Instead, the latter tissues contain large neurites filled with pleomorphic features of smooth endoplasmic reticulum. Arrows indicate abnormal neuritic structures, some of which are magnified in d, e, and f. Bars, 1 μm.

analyses clearly revealed the lack of Purkinje cells in the cerebellum (Figure 6C) and large pyramidal neurons in both the cerebral cortex (Figure 6A) and hippocampus (Figure 6B) of $Atg7^{F/F}$:Nes:$p62^{-/-}$ as well as $Atg7^{F/F}$:Nes mice. We also found a number of eosinophilic spheroids in H&E-stained sections in the cerebellar nuclei of $Atg7^{F/F}$:Nes:$p62^{-/-}$ mice, similar to $Atg7^{F/F}$:Nes mice (Figure 6C). A marked increase in the number of TUNEL (terminal deoxynucleotidyl transferase [TdT]-mediated dUTP-biotin nick end labeling)-positive cells, which were noted in both $Atg7^{F/F}$:Nes cerebral cortices and granular cell layers of the cerebellum at P28, tended to decrease in similar regions of $Atg7^{F/F}$:Nes:$p62^{-/-}$ mice (Figures 6D and 6E), albeit statistically insignificant. Thus, these results indicate that ablation of *p62* does not result in improvement or exacerbation of the phenotypes in autophagy-deficient neurons.

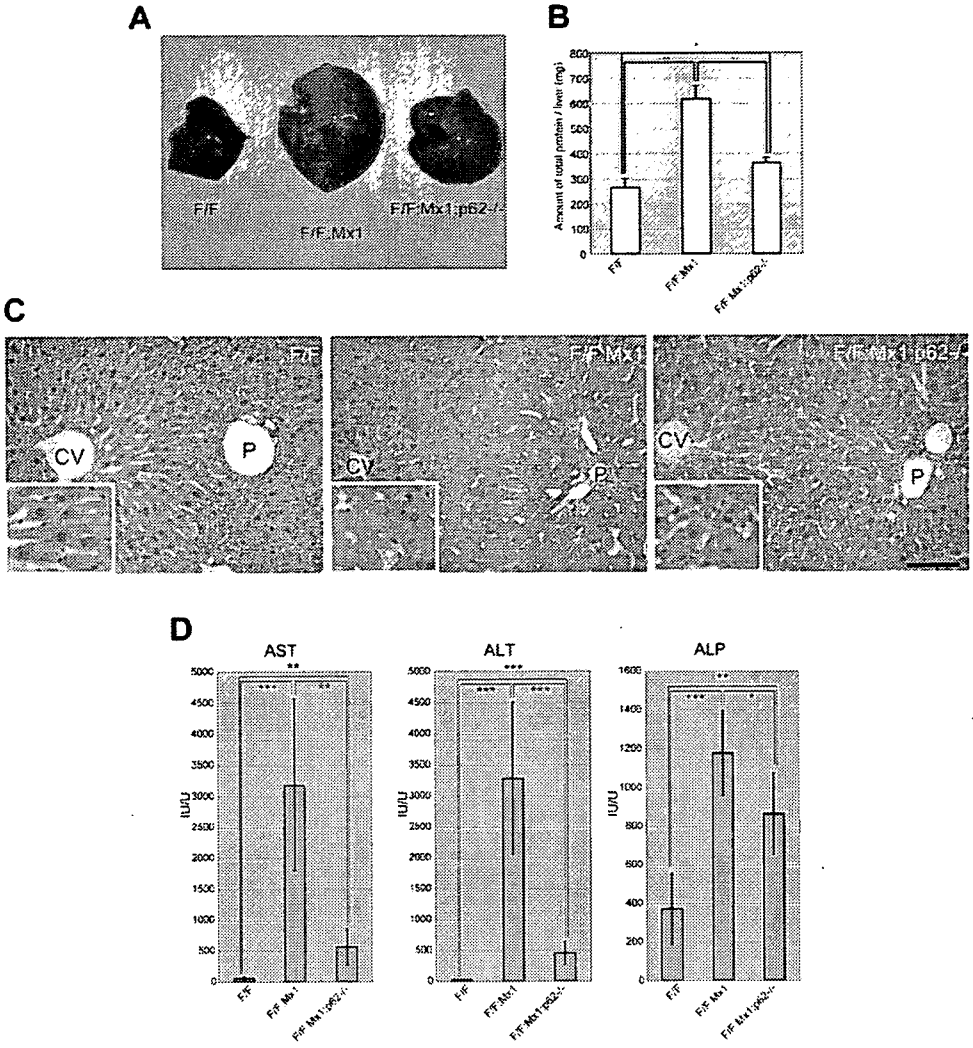

Figure 5. Suppression of Liver Dysfunction in Autophagy-Deficient Mice by Additional Loss of *p62*

(A) Gross anatomical views of representative livers from mice of the indicated genotype at 28-day post-pIpC injection.

(B) Amount of total liver protein. Livers from mice shown in (A) were dissected out, and amounts of total protein per liver were measured. Data are mean ± SD values of five mice in each group. $^{*}p < 0.05$, $^{**}p < 0.01$, and $^{***}p < 0.001$ (Student's t test).

(C) Typical histology of livers from mice of the indicated genotype. H&E staining of respective livers was conducted at 56-day post-pIpC injection. Higher magnification views are shown in insets. CV, central vein; P, portal vein. Bar, 100 μm.

(D) Liver function tests of mice shown in (A). Serum levels of AST, ALT, and ALP were measured. Data represent mean ± SD values of seven mice in each group. $^{*}p < 0.05$, $^{**}p < 0.01$, and $^{***}p < 0.001$.

Aberrant Accumulation of p62 Induces Detoxifying Enzymes in Livers but Not in Brains

Our data clearly showed that loss of *p62* suppresses liver dysfunction but not neurodegeneration in autophagy-deficient mice. How does p62 function differently in autophagy-deficient liver and brain? To elucidate the underlying mechanism for the difference, we examined gene-expression profiles in autophagy-deficient mice by microarray analyses and found that detoxifying enzymes including glutathione S-transferase (GST) families, cytochrome P450 families, and NAD(P)H dehydrogenase quinone 1 (Nqo1) were highly expressed in the autophagy-deficient liver. However, none of these detoxifying enzymes was upregulated in the autophagy-deficient brain (Figure 7A). Moreover, such induction in the liver was suppressed almost completely by additional loss of *p62* (Figure 7A). As shown in Figure 2D, accumulation and insolubilization of both p62 and ubiquitinated proteins began at 4 days post-pIpC injection in *Atg7*$^{F/F}$:Mx1 liver. Furthermore, upregulation of detoxifying enzymes began at 8 days and reached a plateau at 12 days post-pIpC injection (Figure 7B). Meanwhile, significant leakage of ALT and AST, representing hepatocyte death, occurred at later time points (Figure 7C), suggesting that the increase of detoxifying enzymes was not a secondary effect of liver dysfunction.

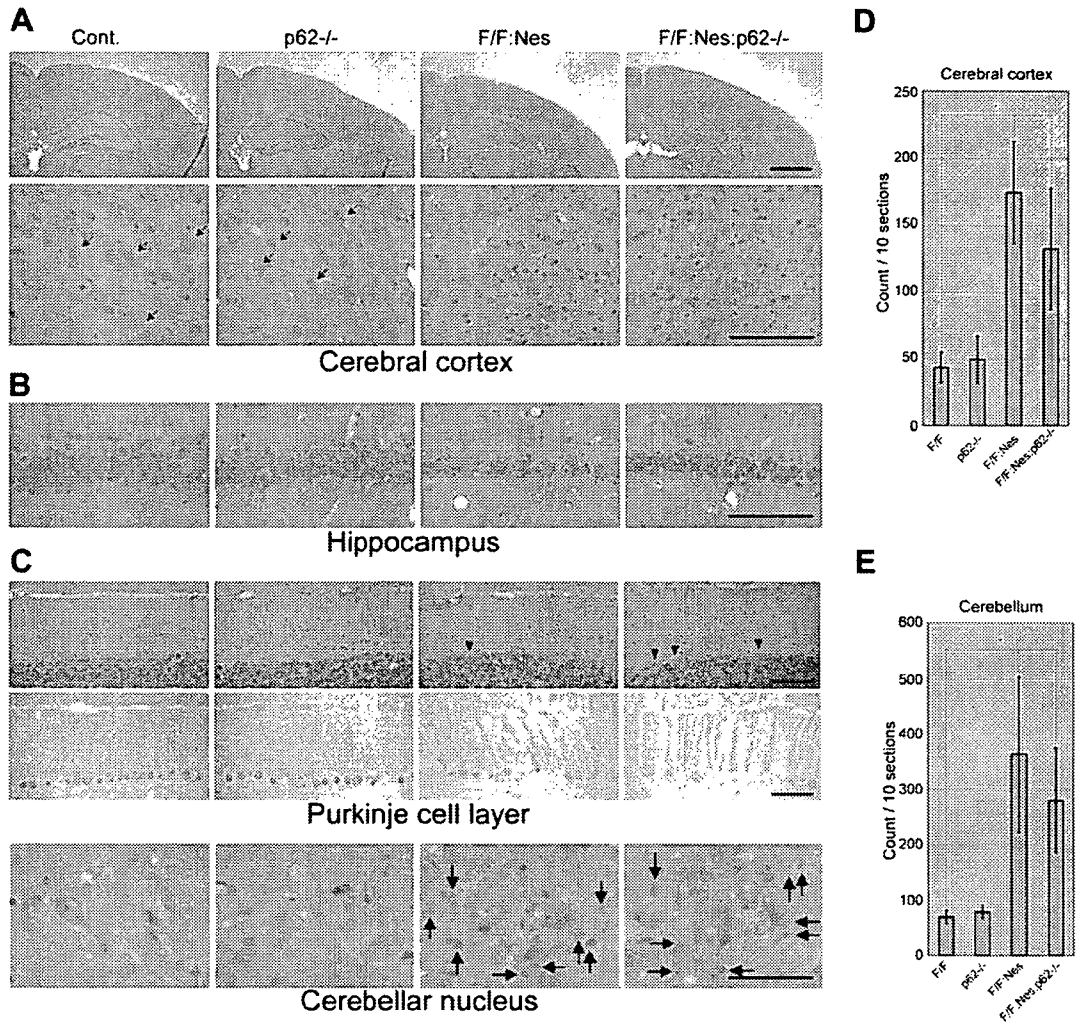

Figure 6. Ablation of *p62* Leads to Neither Improvement nor Exacerbation of the Phenotypes in Autophagy-Deficient Neurons

(A and B) H&E staining of the cerebral cortex (A) and pyramidal cell layer of the hippocampus (B) in mice of the indicated genotype at 4 weeks of age. Top panels in (A) are magnified in bottom panels. Arrows in (A) point to large pyramidal neurons in the cerebral cortex.

(C) Histological analysis of the cerebellar cortex (top and middle panels) and cerebellar nucleus (bottom panel). Cryosections from 8-week-old mice were stained with H&E (top and bottom panels) or immunostained with Purkinje cell marker, calbindin (middle panels). Bars, 1 mm (A, top panel), 200 μm (C, bottom panel), 100 μm (A, bottom panel), (B and C, top and middle panels).

(D and E) Apoptotic cells in the cerebral cortex (D) and cerebellum (E) at 8 weeks of age of the indicated four genotypes. Bars represent the average number (±SD) of total TUNEL-positive cells in ten sections counted in three animals for each genotype. *$p < 0.05$.

A key question is how such enzymes are specifically induced in the autophagy-deficient liver. To this end, we examined the behavior of the transcriptional factor "Nrf2," which translocates to the nucleus in response to oxidative and electrophilic stresses to activate the transcription of various detoxifying enzymes including Gstm1 and Nqo1 (Tong et al., 2006). As shown in Figure 7D, the level of Nrf2 was markedly higher in the nuclear fraction from *Atg7*$^{F/F}$:Mx1 liver but very low in those from control and *p62*-knockout livers. Importantly, the translocation of Nrf2 into the nucleus in *Atg7*$^{F/F}$:Mx1 liver was almost completely suppressed by additional loss of *p62*, implying that autophagy-deficiency causes cellular stress in the liver, which negatively affects hepatocyte function and concomitantly induces p62-dependent activation of Nrf2.

DISCUSSION

p62 Handles Formation of Cytoplasmic Inclusions

While there is ample evidence that dysfunction of the ubiquitin-proteasome system leads to the formation of ubiquitin-positive inclusions, which are the pathological hallmark of various neurodegenerative diseases (Goldberg, 2003), suppression of autophagy also leads to the formation of ubiquitin-positive inclusion (Hara et al., 2006; Komatsu et al., 2005, 2006). However, the molecular mechanism(s) involved in the formation of these inclusions is not clear to

date. In the present study, we found marked accumulation of p62 and ubiquitinated proteins and subsequent inclusion formation in *Atg7*-deficient mice (Figures 2 and 3). Intriguingly, p62 has been identified as a major component of ubiquitin-containing inclusions known as the "hepatocytic Mallory body" found in alcoholic hepatitis and steatohepatitis (Stumptner et al., 2002). Similar inclusions have been also recognized frequently in proteinaceous aggregates in the remnant neurons in various neurodegenerative disorders such as Parkinson's disease and amyotrophic lateral sclerosis (Kuusisto et al., 2001; Nakano et al., 2004). In such diseases, it is plausible that the reduced autophagic activity may be associated with the generation of inclusion bodies.

Surprisingly, loss of *p62* was associated with marked reduction of ubiquitin-positive inclusions, which were otherwise abundantly present in *Atg7*-deficient hepatocytes and neurons (Figure 4). Because ubiquitin-tagged proteins are sticky but do not exhibit aggregation-prone nature themselves, the high levels of p62 due to impaired autophagy might predispose to inclusion formation via the PB1 domain, which retains the ability of self oligomerization (Lamark et al., 2003). Indeed, overexpression of p62 forms inclusions, which is dependent on the presence of both PB1 and UBA domains (Bjorkoy et al., 2005). Since almost all inclusions in autophagy-deficient cells were positive for both ubiquitin and p62, it is possible that ubiquitinated proteins initially interact with p62, and subsequently the protein complex becomes inclusions in a p62-dependent manner. Although autophagy is involved in protection from several discrete diseases (Fortun et al., 2003; Kamimoto et al., 2006; Ravikumar et al., 2004), whether p62 is indeed essential for the formation of disease-related inclusions or not remains unknown at present. However, intriguingly, the formation of ubiquitin-positive aggregates induced by proteasome inhibition is greatly suppressed in *p62*-deficient cells (Wooten et al., 2006), suggesting that p62 is a general mediator of inclusion formation.

p62-Dependent Liver Impairment in Autophagy-Deficient Mice

Our present studies suggest that the pathological changes in *Atg7*-deficient liver are due, at least in part, to oxidative stress associated with proteinaceous aggregates formed by excess accumulation of p62 and ubiquitinated proteins. However, emerging evidence indicates that protein aggregates containing disease-related proteins (e.g., polyQ) can provide protection (Arrasate et al., 2004; Ross and Poirier, 2005; Sanchez et al., 2003). Similarly, aggregate formation mediated by p62 seems to be a protective mechanism in the presence of overexpression of polyQ (Bjorkoy et al., 2005). Therefore, p62 might play an important role in the surveillance of protein abnormalities by adaptively segregating ubiquitin-tagged toxic proteins as inclusions in cells. It is noteworthy that oligomer and protofibrillar intermediates, which are cytotoxic (Arrasate et al., 2004; Ross and Poirier, 2005; Sanchez et al., 2003), must form before the formation of harmless aggregates and generate reactive oxygen species, which are the primary mediators of oxidative stress (Tabner et al., 2005). Because genetic ablation of autophagy in the liver causes exhaustive accumulation of both p62 and ubiquitinated proteins, the liver might show mixed symptoms related to the cytotoxic effects and protective reactions—i.e., continuous formation of both "harmful oligomer and protofibrillar intermediates" and "harmless aggregates" and induction of both "oxidative stress" and "detoxifying enzymes." According to this scenario, simultaneous loss of p62 under autophagy-deficient background might attenuate accumulation of unfavorable harmful oligomer and protofibrillar intermediates, which ultimately form harmless inclusion, leading to alleviation of liver injury.

In this context, we found that impairment of liver autophagy led to nuclear translocation of Nrf2 (Figure 7D), which is responsible for inducible transcription of various antioxidant and detoxifying enzymes, providing mechanistic insights into the upregulation of those enzymes in the autophagy-deficient liver. In the absence of stress, Nrf2 is constitutively degraded through the ubiquitin-proteasome pathway, since the binding partner Keap1 is a ubiquitin-protein ligase. Exposure to oxidative and electrophilic insults results in modification of Cys residues of Keap1, and leads to inactivation of Keap1. Stabilization of Nrf2 leads to its nuclear translocation to induce the transcription of detoxifying enzymes (Tong et al., 2006). Accordingly, we surmise that the autophagy-deficient liver may be filled with oxidative and/or other Nrf2-inducing stresses. More interestingly, simultaneous loss of *p62* and *Atg7* completely suppressed the translocation of Nrf2 (Figure 7D). These results strongly argue for accumulation of cellular stress in autophagy-deficient liver, the extent of which depends on the impairment of p62 turnover, and they shed light on the mechanism of p62 loss-associated attenuation of autophagy-deficiency-related liver injury.

On the other hand, leakage of hepatocytic enzymes into peripheral blood still occurred at a significantly high level in $Atg7^{F/F}$:Mx1:$p62^{-/-}$ compared with control mice (Figure 5D), implying other abnormalities apart from p62 accumulation in the DKO livers. In fact, in addition to accumulation of soluble ubiquitinated proteins, impairment of organelle turnover was not rescued by the additional defect of *p62* (Figures 4B and 4C). Such abnormalities together with the excess accumulation of p62 might have irreversible cytotoxic effects in autophagy-deficient hepatocytes.

p62-Independent Neuronal Death in Autophagy-Deficient Mice

Unlike the liver, the survival of *Atg7*-deficient neurons is affected little when *p62* is abolished, although p62 can form protein aggregates in neuronal cells as in hepatocytes. This paradoxical observation may underlie the difference in autophagic activity among cell-types or tissues. The constitutive autophagic activity in the brain is low compared

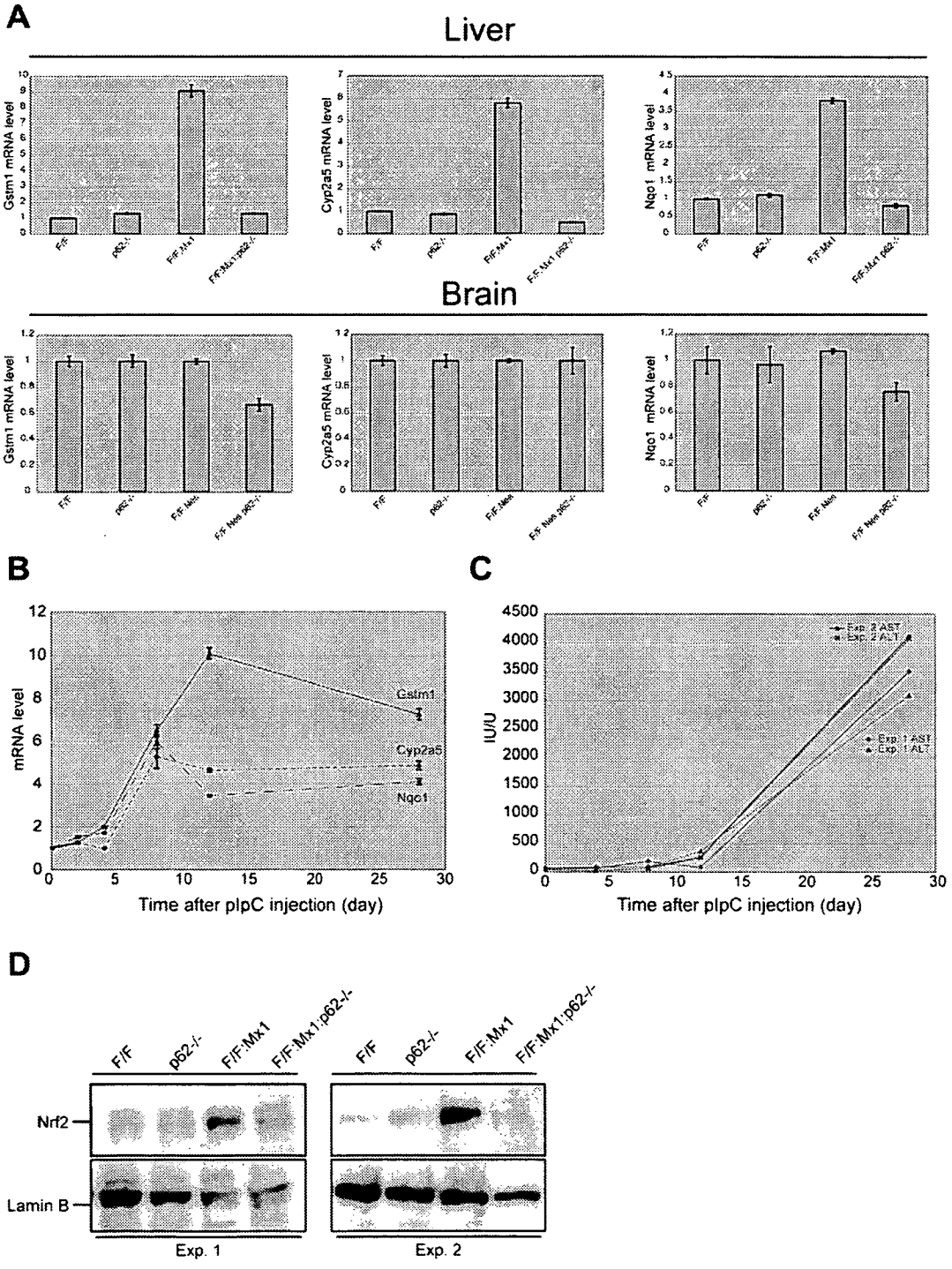

Figure 7. p62-Dependent Induction of Detoxifying Enzymes in Autophagy-Deficient Liver but Not in Brain

(A) Quantitative RT-PCR analyses of Gstm1, Cy2a5, and Nqo1 in mouse liver (top panels) and brain (bottom panels). Total RNAs were prepared from the livers of the indicated genotypes at 12 days post-pIpC injection and brains of the indicated genotypes at postnatal day 28. The values are normalized to the amount of mRNA in $Atg7^{F/F}$ liver and brain. The experiments were performed three times.

(B) Quantitation of mRNA levels of detoxifying enzymes in $Atg7^{F/F}$:Mx1 liver by RT-PCR. Total RNAs were prepared from $Atg7^{F/F}$:Mx1 mice livers at various time points post-pIpC injection, and then cDNA was synthesized from each RNA, followed by real-time PCR analyses. The values are normalized to the amount of each mRNA in $Atg7^{F/F}$:Mx1 liver at 0 days post-pIpC injection.

(C) Liver function tests of mice at various time points post-pIpC injection. Serum levels of AST and ALT were measured in $Atg7^{F/F}$:Mx1 mice. Data represent two independent mice.

with other tissues such as the liver (Mizushima et al., 2004). Accordingly, significant accumulation of ubiquitinated proteins was noted in *Atg7*-deficient brain, but their levels, especially insoluble ubiquitinated proteins, were lower than in *Atg7*-deficient liver (Figures 4E and S10B), and severe formation of the inclusion was found in restricted groups of neurons (Figures 4D and S8). Moreover, unlike in the liver, detoxifying enzymes did not increase in *Atg7*-deficient brain (Figure 7A), suggesting the low susceptibility of neurons to toxicity associated with aggregate formation. In fact, several ubiquitin-positive aggregates were recognized in *Atg7*-deficient brain regions in the presence of mild neuronal loss (Komatsu et al., 2006).

Why do autophagy-deficient mice develop neurodegeneration? Analyses of Purkinje cell-specific *Atg7*-knockout mice demonstrated that *Atg7*-deficient Purkinje cells initially causes cell-autonomous, progressive dystrophy (manifested by axonal swelling) and degeneration of the axon terminals followed by cell-autonomous Purkinje cell death and mouse behavioral deficits (Komatsu et al., 2007). The mutant Purkinje cells developed aberrant organelles in the swelling axons, suggesting the important role of autophagy in the regulation of local axonal membrane trafficking and turnover, and implicate impairment of axonal autophagy as a mechanism for axonopathy associated with neurodegeneration. Importantly, such axonopathy in *Atg7*-deficient Purkinje cells and hypothalamic neurons was still observed in *Atg7/p62*-DKO neurons (Figures 4F, 6C, and S12), indicating that the development of axonopathy in *Atg7*-deficient neurons is *p62* independent. Therefore, we hypothesize that the mechanism of neurodegeneration caused by autophagy deficiency might involve distinct pathogenic pathways, such as axonal dystrophy and degeneration.

EXPERIMENTAL PROCEDURES

Generation of Knockout Mice

Atg7$^{F/F}$:Mx1 mice (Komatsu et al., 2005) were bred with GFP-LC3 Tg mice (Mizushima et al., 2004) to generate *Atg7*$^{F/F}$:Mx1:GFP-LC3 mice. *p62*$^{-/-}$ mice were bred with *Atg7*$^{F/F}$:Mx1, *Atg7*$^{F/F}$:Mx1:GFP-LC3, and *Atg7*$^{F/F}$:Nes mice (Komatsu et al., 2006) to generate *Atg7*$^{F/F}$:Mx1:*p62*$^{-/-}$, *Atg7*$^{F/F}$:Mx1:*p62*$^{-/-}$:GFP-LC3, and *Atg7*$^{F/F}$:Nes:*p62*$^{-/-}$ mice, respectively. With regard to deletion of *Atg7* from the liver, Cre expression in the liver was induced by intraperitoneal injection of pIpC (Sigma Chemical Co., St. Louis, MO) (Komatsu et al., 2005). Mice were housed in specific-pathogen-free facilities, and the experimental protocol was approved by the Ethics Review Committee for Animal Experimentation of Tokyo Metropolitan Institute of Medical Science. Other mice strains shown in Supplemental Data are described in Supplemental Experimental Procedures.

Immunological Analysis

Livers and brains were homogenized in 0.25 M sucrose, 10 mM 2-[4-(2-hydroxyethyl)-1-piperazinyl]ethanesulfonic acid [HEPES], pH 7.4, and 1 mM dithiothreitol (DTT). The resultant homogenates were fractionated into 0.5% Tx-100 soluble and insoluble fractions. Immunoprecipitation and immunoblot analyses were conducted as described previously (Komatsu et al., 2004). Nuclear fraction from the liver was prepared according to the method of Blobel and Potter (Blobel and Potter, 1966). The antibodies for p62, Atg7, and LC3 were described previously (Ishii et al., 1996; Komatsu et al., 2005). The antibodies for GFP (Medical and Biological Laboratories [MBL] Co., Nagoya, Japan), ubiquitin (FK2; MBL), Nrf2 (H-300: Santa Cruz Biotechnology, Inc., Santa Cruz, CA), LDH (ab2101: abcam, Inc., Cambridge, MA), actin (MAB1501R: Chemicon International, Inc., Temecula, CA) and Lamin B (M-20: Santa Cruz Biotechnology, Inc.) were purchased.

Pull-Down Assay

Recombinant GST, GST-LC3, and GST-p62 were produced in *Escherichia coli*, and recombinant proteins were purified by chromatography on glutathione-Sepharose 4B (Amersham Biosciences, Arlington Heights, IL). The GST-p62 cleaved the GST tag by precision protease (Amersham Biosciences). Purified p62 and GST or GST-LC3 were mixed in TNE buffer (Komatsu et al., 2004) for 3 hr at 4°C and then precipitated with glutathione-Sepharose. The mixtures were washed five times with ice-cold TNE. The bound proteins were analyzed by SDS-PAGE followed by Coomassie brilliant blue (CBB) staining.

Quantitative RT-PCR

cDNA was synthesized from 1 μg of total RNA using the Transcriptor First Strand cDNA Synthesis Kit (Roche Applied Science), and quantitative PCR was performed using LightCycler 480 Probes Masterin (Roche Applied Science) in a LightCycler 480 (Roche Applied Science). Signals were normalized to β-glucronidase (GUS). Primer sequences are described in Supplemental Experimental Procedures.

Immunofluorescence Microscopy of Cultured Hepatocytes

Hepatocytes grown on glass coverslips were immunostained with anti-p62 or ubiquitin (DakoCytomation, Glostrup, Denmark) antibody as described previously (Komatsu et al., 2005). The coverslips were mounted and viewed with a laser-scanning confocal microscope (FV1000, Olympus) or conventional epifluorescent microscope.

Histological Examination

Methods for tissue fixation and subsequent procedures, including H&E staining, immunohistochemistry, conventional electron microscopy, immunoelectron microscopy, and TUNEL staining were described previously (Komatsu et al., 2005, 2006). Antibodies used for immunohistochemistry and immunoelectron microscopy were as follows: rabbit polyclonal antibodies against LC3 (Komatsu et al., 2005), p62 (Ishii et al., 1996), and GFP (Abcam), and mouse monoclonal antibodies against ubiquitin (FK2 and 1B3: MBL).

Statistical Analysis

Data were analyzed by two-tailed Student's t test. For all graphs, data are represented as mean ± SD.

Supplemental Data

Supplemental Data include 13 figures, 1 table, Supplemental Experimental Procedures, and Supplemental References and can be found with this article online at http://www.cell.com/cgi/content/full/131/6/1149/DC1/.

ACKNOWLEDGMENTS

We thank T. Kaneko, T. Kouno, and K. Tatsumi for the excellent technical assistance. We also thank F. Kaji, K. Kanno, and A. Yabashi for their help in electron microscopy study and M. Kasahara for the phylogenetic tree analysis. This work was supported by grants from the

(D) The level of Nrf2 in liver nuclear fraction. Nuclear fractions were prepared from liver of the indicated genotypes at 12 days post-pIpC injection, subjected to SDS-PAGE, and analyzed by immunoblotting with antibodies against Nrf2 and Lamin B (as a control). Data represent two independent mice.

Japan Science and Technology Agency (M.K.) and the Ministry of Education, Science and Culture of Japan (M.K. and K.T.).

Received: January 5, 2007
Revised: June 26, 2007
Accepted: October 9, 2007
Published: December 13, 2007

REFERENCES

Arrasate, M., Mitra, S., Schweitzer, E.S., Segal, M.R., and Finkbeiner, S. (2004). Inclusion body formation reduces levels of mutant huntingtin and the risk of neuronal death. Nature *431*, 805–810.

Bjorkoy, G., Lamark, T., Brech, A., Outzen, H., Perander, M., Overvatn, A., Stenmark, H., and Johansen, T. (2005). p62/SQSTM1 forms protein aggregates degraded by autophagy and has a protective effect on huntingtin-induced cell death. J. Cell Biol. *171*, 603–614.

Blobel, G., and Potter, V.R. (1966). Nuclei from rat liver: isolation method that combines purity with high yield. Science *154*, 1662–1665.

Elmore, S.P., Qian, T., Grissom, S.F., and Lemasters, J.J. (2001). The mitochondrial permeability transition initiates autophagy in rat hepatocytes. FASEB J. *15*, 2286–2287.

Fortun, J., Dunn, W.A., Jr., Joy, S., Li, J., and Notterpek, L. (2003). Emerging role for autophagy in the removal of aggresomes in Schwann cells. J. Neurosci. *23*, 10672–10680.

Goldberg, A.L. (2003). Protein degradation and protection against misfolded or damaged proteins. Nature *426*, 895–899.

Hara, T., Nakamura, K., Matsui, M., Yamamoto, A., Nakahara, Y., Suzuki-Migishima, R., Yokoyama, M., Mishima, K., Saito, I., Okano, H., and Mizushima, N. (2006). Suppression of basal autophagy in neural cells causes neurodegenerative disease in mice. Nature *441*, 885–889.

Ichimura, Y., Kirisako, T., Takao, T., Satomi, Y., Shimonishi, Y., Ishihara, N., Mizushima, N., Tanida, I., Kominami, E., Ohsumi, M., et al. (2000). A ubiquitin-like system mediates protein lipidation. Nature *408*, 488–492.

Ishii, T., Yanagawa, T., Kawane, T., Yuki, K., Seita, J., Yoshida, H., and Bannai, S. (1996). Murine peritoneal macrophages induce a novel 60-kDa protein with structural similarity to a tyrosine kinase p56lck-associated protein in response to oxidative stress. Biochem. Biophys. Res. Commun. *226*, 456–460.

Iwata, J., Ezaki, J., Komatsu, M., Yokota, S., Ueno, T., Tanida, I., Chiba, T., Tanaka, K., and Kominami, E. (2006). Excess peroxisomes are degraded by autophagic machinery in mammals. J. Biol. Chem. *281*, 4035–4041.

Kabeya, Y., Mizushima, N., Ueno, T., Yamamoto, A., Kirisako, T., Noda, T., Kominami, E., Ohsumi, Y., and Yoshimori, T. (2000). LC3, a mammalian homologue of yeast Apg8p, is localized in autophagosome membranes after processing. EMBO J. *19*, 5720–5728.

Kamimoto, T., Shoji, S., Hidvegi, T., Mizushima, N., Umebayashi, K., Perlmutter, D.H., and Yoshimori, T. (2006). Intracellular inclusions containing mutant alpha1-antitrypsin Z are propagated in the absence of autophagic activity. J. Biol. Chem. *281*, 4467–4476.

Komatsu, M., Chiba, T., Tatsumi, K., Iemura, S., Tanida, I., Okazaki, N., Ueno, T., Kominami, E., Natsume, T., and Tanaka, K. (2004). A novel protein-conjugating system for Ufm1, a ubiquitin-fold modifier. EMBO J. *23*, 1977–1986.

Komatsu, M., Waguri, S., Ueno, T., Iwata, J., Murata, S., Tanida, I., Ezaki, J., Mizushima, N., Ohsumi, Y., Uchiyama, Y., et al. (2005). Impairment of starvation-induced and constitutive autophagy in Atg7-deficient mice. J. Cell Biol. *169*, 425–434.

Komatsu, M., Waguri, S., Chiba, T., Murata, S., Iwata, J., Tanida, I., Ueno, T., Koike, M., Uchiyama, Y., Kominami, E., and Tanaka, K. (2006). Loss of autophagy in the central nervous system causes neurodegeneration in mice. Nature *441*, 880–884.

Komatsu, M., Wang, Q.J., Holstein, G.R., Friedrich, V.L., Iwata, J.I., Kominami, E., Chait, B.T., Tanaka, K., and Yue, Z. (2007). Essential role for autophagy protein Atg7 in the maintenance of axonal homeostasis and the prevention of axonal degeneration. Proc. Natl. Acad. Sci. USA *104*, 14489–14494.

Kuma, A., Hatano, M., Matsui, M., Yamamoto, A., Nakaya, H., Yoshimori, T., Ohsumi, Y., Tokuhisa, T., and Mizushima, N. (2004). The role of autophagy during the early neonatal starvation period. Nature *432*, 1032–1036.

Kuusisto, E., Salminen, A., and Alafuzoff, I. (2001). Ubiquitin-binding protein p62 is present in neuronal and glial inclusions in human tauopathies and synucleinopathies. Neuroreport *12*, 2085–2090.

Lamark, T., Perander, M., Outzen, H., Kristiansen, K., Overvatn, A., Michaelsen, E., Bjorkoy, G., and Johansen, T. (2003). Interaction codes within the family of mammalian Phox and Bem1p domain-containing proteins. J. Biol. Chem. *278*, 34568–34581.

Levine, B., and Klionsky, D.J. (2004). Development by self-digestion: molecular mechanisms and biological functions of autophagy. Dev. Cell *6*, 463–477.

Mizushima, N., Yamamoto, A., Hatano, M., Kobayashi, Y., Kabeya, Y., Suzuki, K., Tokuhisa, T., Ohsumi, Y., and Yoshimori, T. (2001). Dissection of autophagosome formation using Apg5-deficient mouse embryonic stem cells. J. Cell Biol. *152*, 657–668.

Mizushima, N., Yamamoto, A., Matsui, M., Yoshimori, T., and Ohsumi, Y. (2004). In vivo analysis of autophagy in response to nutrient starvation using transgenic mice expressing a fluorescent autophagosome marker. Mol. Biol. Cell *15*, 1101–1111.

Moscat, J., Diaz-Meco, M.T., Albert, A., and Campuzano, S. (2006). Cell signaling and function organized by PB1 domain interactions. Mol. Cell *23*, 631–640.

Nakano, T., Nakaso, K., Nakashima, K., and Ohama, E. (2004). Expression of ubiquitin-binding protein p62 in ubiquitin-immunoreactive intraneuronal inclusions in amyotrophic lateral sclerosis with dementia: analysis of five autopsy cases with broad clinicopathological spectrum. Acta Neuropathol. (Berl.) *107*, 359–364.

Ohsumi, Y. (2001). Molecular dissection of autophagy: two ubiquitin-like systems. Nat. Rev. Mol. Cell Biol. *2*, 211–216.

Ravikumar, B., Vacher, C., Berger, Z., Davies, J.E., Luo, S., Oroz, L.G., Scaravilli, F., Easton, D.F., Duden, R., O'Kane, C.J., and Rubinsztein, D.C. (2004). Inhibition of mTOR induces autophagy and reduces toxicity of polyglutamine expansions in fly and mouse models of Huntington disease. Nat. Genet. *36*, 585–595.

Rodriguez, A., Duran, A., Selloum, M., Champy, M.F., Diez-Guerra, F.J., Flores, J.M., Serrano, M., Auwerx, J., Diaz-Meco, M.T., and Moscat, J. (2006). Mature-onset obesity and insulin resistance in mice deficient in the signaling adapter p62. Cell Metab. *3*, 211–222.

Ross, C.A., and Poirier, M.A. (2005). Opinion: What is the role of protein aggregation in neurodegeneration? Nat. Rev. Mol. Cell Biol. *6*, 891–898.

Sanchez, P., De Carcer, G., Sandoval, I.V., Moscat, J., and Diaz-Meco, M.T. (1998). Localization of atypical protein kinase C isoforms into lysosome-targeted endosomes through interaction with p62. Mol. Cell. Biol. *18*, 3069–3080.

Sanchez, I., Mahlke, C., and Yuan, J. (2003). Pivotal role of oligomerization in expanded polyglutamine neurodegenerative disorders. Nature *421*, 373–379.

Stumptner, C., Fuchsbichler, A., Heid, H., Zatloukal, K., and Denk, H. (2002). Mallory body–a disease-associated type of sequestosome. Hepatology *35*, 1053–1062.

Tabner, B.J., El-Agnaf, O.M., German, M.J., Fullwood, N.J., and Allsop, D. (2005). Protein aggregation, metals and oxidative stress in neurodegenerative diseases. Biochem. Soc. Trans. *33*, 1082–1086.

Tong, K.I., Kobayashi, A., Katsuoka, F., and Yamamoto, M. (2006). Two-site substrate recognition model for the Keap1-Nrf2 system: a hinge and latch mechanism. Biol. Chem. *387*, 1311–1320.

Tsukada, M., and Ohsumi, Y. (1993). Isolation and characterization of autophagy-defective mutants of Saccharomyces cerevisiae. FEBS Lett. *333*, 169–174.

Wang, Q.J., Ding, Y., Kohtz, D.S., Mizushima, N., Cristea, I.M., Rout, M.P., Chait, B.T., Zhong, Y., Heintz, N., and Yue, Z. (2006). Induction of autophagy in axonal dystrophy and degeneration. J. Neurosci. *26*, 8057–8068.

Wooten, M.W., Hu, X., Babu, J.R., Seibenhener, M.L., Geetha, T., Paine, M.G., and Wooten, M.C. (2006). Signaling, polyubiquitination, trafficking, and inclusions: Sequestosome 1/p62's role in neurodegenerative disease. J. Biomed. Biotechnol. *2006*, 62079.

Acta Neurol Scand 2007: 116: 340–344 DOI: 10.1111/j.1600-0404.2007.00876.x

ACTA NEUROLOGICA
SCANDINAVICA

Constant blood flow reduction in premotor frontal lobe regions in ALS with dementia – a SPECT study with 3D-SSP

Ishikawa T, Morita M, Nakano I. Constant blood flow reduction in premotor frontal lobe regions in ALS with dementia – a SPECT study with 3D-SSP.
Acta Neurol Scand 2007: 116: 340–344.

Objectives – We investigated the regional cerebral blood flow in amyotrophic lateral sclerosis with dementia (ALS-D) patients, using single photon emission computed tomography (SPECT). *Materials and methods* – The ^{123}I-IMP SPECT data for 5 ALS-D and 16 ALS patients were analyzed using three-dimensional stereotactic surface projection (3D-SSP). *Results* – 3D-SSP demonstrated marked prefrontal hypoperfusion in all the five ALS-D cases and significant bilateral prefrontal hypoperfusion in group comparisons. *Conclusions* – This study revealed prefrontal hypoperfusion in ALS-D cases to be an obvious abnormality with scientific objectivity.

T. Ishikawa, M. Morita, I. Nakano

Division of Neurology, Department of Internal Medicine, Jichi Medical University, Tochigi, Japan

Key words: amyotrophic lateral sclerosis with dementia; premotor frontal lobe region; regional cerebral blood flow; single photon emission computed tomography; three-dimensional stereotactic surface projection

Mitsuya Morita, Division of Neurology, Department of Internal Medicine, Jichi Medical University, 3311-1 Yakushiji, Shimotsuke, Tochigi 329 0498, Japan
Tel.: +81 285 58 7352
Fax: +81 285 44 5118
e-mail: morita@jichi.ac.jp

Accepted for publication March 25, 2007

Introduction

Amyotrophic lateral sclerosis (ALS) is a degenerative disorder that involves progressive muscle weakness, and the lesions are essentially restricted to upper and lower motor neurons. Traditionally, patients with ALS have been recognized to be free from cognitive impairment. Evidence is emerging, however, that the cognitive function is impaired in some ALS patients, and such cases have been repeatedly described, especially in Japan (1).

Single photon emission computed tomography (SPECT) studies have been performed for the evaluation of the regional cerebral blood flow (rCBF) in various neurodegenerative disorders, including ALS and ALS-D. Such studies revealed cortical hypoperfusion in the premotor frontal lobe cortex and/or motor cortex in ALS (2, 3) or ALS with dementia (ALS-D) (4, 5), leading the researchers to state that ALS-D is included in the spectrum of ALS (6). The reported hypoperfusion in these regions, however, lacked objectivity, because the SPECT data were not standardized. With recent advances in computer-assisted analysis of SPECT images using three-dimensional stereotactic surface projection (3D-SSP) (7, 8), we have become able to detect a slight change in rCBF with scientific objectivity. Nevertheless, there have been few studies to discriminate subjects with ALS-D from non-demented ALS cases using such statistical methods. The purpose of this study was to evaluate rCBF in ALS-D and ALS cases using an objective and accurate method for analysis such as 3D-SSP, and to discuss the relationship between ALS-D and classic ALS.

Material and methods

Cases

Forty-one ALS cases had been diagnosed in the Neurology Department of Jichi Medical University from 1997 to 2003, five of whom had dementia. Among them, 16 ALS patients and five ALS with dementia patients could be evaluated by SPECT. Five ALS-D (two men and three women, mean ± SD: 54.8 ± 3.4 years old) and 16 ALS cases (nine men and seven women, mean ± SD: 66.5 ± 11.8 years old) were selected for analysis. The diagnosis of ALS was established according to the El Escorial criteria (9). None of the patients had either symptoms of a cerebrovascular disease or infarcts detectable in CT or MR images.

Table 1 Clinical features of the amyotrophic lateral sclerosis with dementia (ALS-D)

ALS-D cases	Age (years old) /Sex	The duration of illness at the time of SPECT (months)	Initial symptom	HDS-R	WAIS-R	Loss of memory	Insight into disease	Personality change /Emotional disorder	Autopsy
ALS-D 1	58/F	8	Memory loss	19	N/A	+	−	+	−
ALS-D 2	50/M	8	Memory loss	N/A	Verbal (57) Performance (51) Full (47)	+	−	+	+
ALS-D 3	59/F	19	Upper limb weakness	22	Verbal (100) Performance (75) Full (89)	−	−	+	+
ALS-D 4	52/F	27	Paranoia	18	N/A	+	−	+	+
ALS-D 5	55/M	45	Personality change	19	N/A	+	−	+	−
	54.8 ± 3.4 (mean ± SD)	21.4 ± 13.8 (mean ± SD)							
ALS cases									
Total 16 cases	66.5 ± 11.8 (mean ± SD)	21.4 ± 14.7 (mean ± SD)							

When individuals exhibited both ALS and an intellectual impairment constellation, such as loss of memory, personality change, emotional disorder and language impairment (the clinical features are summarized in Table 1), the diagnosis of ALS-D was made. For the evaluation of intellectual impairment, we used the Wechsler Adult Intelligence Scale-Revised (WAIS-R) and/or the revised Hasegawa Dementia Scale (HDS-R). The HDS-R is widely used as a brief cognitive screen instrument in Japan, and the result is known to be correlated well with the Mini-Mental State Examination (MMSE). The low-normal cut off is estimated to be 20, and the results are summarized in Table 1. Two ALS-D cases were also evaluated with the WAIS-R.

Assessment with the WAIS-R yielded a verbal IQ of 57, performance IQ of 51 and full IQ of 47 in case 2, a verbal IQ of 100, performance IQ of 75 and full IQ of 89 in case 3. Case 3 developed limb weakness as an initial symptom, and her intellectual impairment was negligible when she was diagnosed as having ALS, and SPECT study was carried out. Thereafter, she developed prominent dementia.

All the five ALS-D cases finally died of respiratory failure because of motor neuron involvement. Autopsy was performed in three cases (case 2, 3, and 4), and the diagnosis of ALS-D was confirmed according to the result of the autopsy. A total of 33 healthy volunteers (21 men and 12 women, mean ± SD: 58.6 ± 11.0 years old) was used as normal control subjects for 3D-SSP analysis.

SPECT and 3D-SSP

Single photon emission computed tomography with [^{123}I] isopropyl amphetamine (^{123}I-IMP SPECT) image sets was performed. The duration of illness at the time of SPECT was 21.4 ± 13.8 (mean ± SD) months in the ALS-D group and 21.4 ± 14.7 (mean ± SD) months in the ALS one, respectively. We performed 3D-SSP using the Neurological Statistical Image Analysis Software (NEUROSTAT) to evaluate the spatial distribution of an abnormal CBF, (8) and iSSP 35 for Windows to produce single subject *Z*-maps of decreased perfusion in patients. Following stereotactic anatomic standardization, the CBF in an individual's SPECT image set was extracted as a set of predefined surface pixels, which was used in the subsequent analysis. To quantify perfusion deficits, the normalized CBF in each patient was compared with that in 33 normal controls by pixel-by-pixel *Z*-score analysis ([normal mean]-[individual value])/(normal standard deviation; SD). We also compared the intergroup differences between the ALS-D group and normal controls, the ALS-D and ALS groups, and the ALS group and normal controls. A positive *Z*-score represents a reduced CBF in a patient relative to the control mean. In this study, we considered that a *Z*-score of > 3.0 was significant.

Results

The statistical *Z*-scores obtained with 3D-SSP in the ALS-D patients are presented in the Fig. 1.

The reduction of rCBF was consistently prominent and widespread in the middle to inferior areas of the premotor frontal lobe in all five ALS-D patients, while the rCBF decrease in such regions was only subtle and patchy in ALS patients. A mild decrease in the unilateral temporal lobe was also seen in all the five ALS-D patients.

A significant rCBF reduction in the bilateral frontal lobes, especially the premotor frontal lobes,

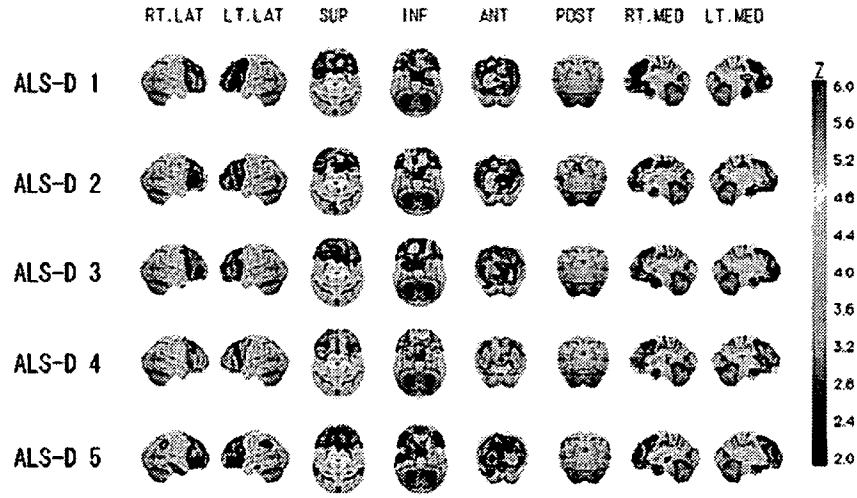

Figure 1. Three-dimensional stereotactic surface projection (3D-SSP) of the amyotrophic lateral sclerosis with dementia (ALS-D) cases compared with normal controls. The *Z*-score images obtained with 3D-SSP demonstrated marked regional cerebral blood flow reduction in the bilateral frontal lobes, especially the prefrontal lobes, in all five ALS-D patients. Images are constructed from eight views [in each line, from left to right, right lateral (RT. LAT), left lateral (LT. LAT), superior (SUP), inferior (INF), anterior (ANT), posterior (POST), right medial (RT. MED), and left medial (LT. MED)].

was evident in the ALS-D group compared with not only in normal controls but also in the ALS group (Fig. 2). One part of the left temporal lobe, the parahippocampal gyrus, also exhibited subtle hypoperfusion in the ALS-D group. On the contrary, in the ALS group, there were subtle rCBF decreases in the anterior part of the cingulate gyrus and the posterior part of the corpus callosum compared with in normal controls. Neither the ALS-D group nor the ALS one exhibited an obvious rCBF reduction in the regions corresponding to the precentral gyrus.

Discussion

Scintigraphical studies have been performed for the evaluation of rCBF in various neurodegenerative disorders, and some researchers have reported cortical hypoperfusion in the frontal cortex and motor cortex in ALS-D (4, 5). In the previous reports, however, as subjective approaches such as visual inspection were used, the reported hypoperfusion in these regions lacked objectivity. The 3D-SSP we used in this study is far superior to the visual inspection method in terms of objectivity. In addition, its sensitivity is reported to be high enough to be able to discriminate patients with a very early stage of the Alzheimer disease from healthy controls (7).

In our study, cortical hypoperfusion in the frontal lobe in the ALS-D group was consistently prominent compared to in the ALS cases, although the mean age of the ALS-D cases was lower than that of the controls or the ALS cases. CBF tends

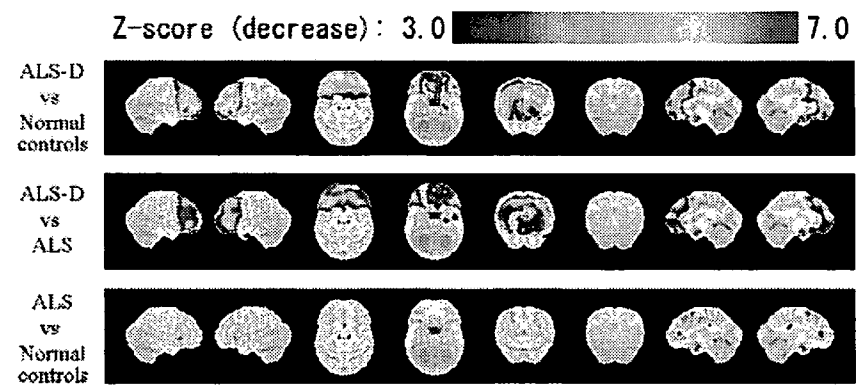

Figure 2. Decrease of regional cerebral blood flow (rCBF) adjusted to the global mean cerebral blood flow using three-dimensional stereotactic surface projection (3D-SSP) in group comparisons. 3D-SSP demonstrated a significant rCBF reduction in the bilateral frontal lobes, especially the prefrontal lobes, in the amyotrophic lateral sclerosis with dementia (ALS-D) group, when compared with either in normal controls or in the ALS group. On the contrary, subtle rCBF decreases in the anterior part of the cingulate gyrus and the posterior part of the corpus callosum were seen in the ALS group when compared with in normal controls. Images are constructed from 8 views in the same order as Fig. 1.